J. Arbocz

Collapse load calculations for axially compressed imperfect stringer stiffened shells

april 1984

Report LR-419

THDelft

Technische Hogeschool Delft

Department of Aerospace Engineering

J. Arbocz

Collapse load calculations for axially compressed imperfect stringer stiffened shells

april 1984

Report LR-419

Department of Aerospace Engineering

ACKNOWLEDGEMENT

The results reported in this paper could not have been obtained without the excellent cooperation of the members of the Digital Production Department of the University Computing Center in Delft. Their help is gratefully acknowledged.

The skilful typing of the manuscript by Mrs. Marlene Lit and the excellent artwork by ir. R.P. Notenboom, Mr. R.H.M. van Boheemen and Mr. L.P.J. Frenken are also very much appreciated,

TABLE OF CONTENTS

LIST OF SYMBOLS

A_1	-	cross-sectional area of stringer
A_{io}	-	axisymmetric coefficient of the Fourier representation used, see Eq. (2)
$A_{o\ell}$, $B_{o\ell}$		
$C_{k\ell}$, $D_{k\ell}$	-	coefficients of the Fourier representation used, see Eq. (2)
d_1	-	stringer spacing
e_1	-	distance between centroid of stringer cross-section and middle surface of skin
E	-	Young's modulus
F.S.	-	factor of safety
i, k	-	number of half-waves in the axial direction
I_{11}	-	moment of inertia of stringer cross-section about its centroidal axis
I_{t_1}	-	torsional modulus of the stringer cross-section
ℓ	-	number of full waves in the circumferential direction
L	-	shell length
M_x	-	moment resultant
N_x	-	stress resultant
R	-	shell radius
t	-	shell wall-thickness
P	-	axial load
$P_{c\ell}$	-	classical buckling load
u, v	-	displacement components in the axial and circumferential directions, respectively
w	-	radial displacement, positive outward
$\bar{w}$	-	radial imperfection from perfect circular cylinder, positive outward
x, y	-	axial and circumferential coordinates on the middle surface of the shell, respectively
Z	-	Batdorf's parameter $(= L^2/Rt\sqrt{1-\nu^2})$
γ	-	"knockdown factor" in Eq. (1)
θ	-	nondimensional circumferential coordinate = Y/R
ρ	-	nondimensional loading parameter
ν	-	Poisson's ratio

COLLAPSE LOAD CALCULATIONS FOR AXIALLY COMPRESSED IMPERFECT STRINGER STIFFENED SHELLS

by

J. Arbocz

ABSTRACT

This paper discusses ways to predict accurately the collapse loads of stringer stiffened shells under axial compression by using the best available nonlinear analysis capability combined with detailed initial imperfection surveys. The numerical analysis is done with a modified version of the STAGS-A computer code. It appears that the buckling load predictions using the measured initial imperfections as input will be within less than 10% of the experimental buckling load if the experimental boundary conditions are modeled correctly.

1. INTRODUCTION

The use of large general purpose computer programs for the analysis of different types of aerospace structures is by now well accepted. These codes have been used successfully to calculate the stress distributions for very complicated structural configurations with the accuracy demanded in engineering analysis. However, when the structure is buckling sensitive, then even today, in 1984, one will often encounter great difficulties in making a reliable prediction for the critical buckling load.

The axially compressed cylindrical shell represents one of the best known examples of the very complicated stability behaviour which can occur with thin-walled constructions. The whole problem is well illustrated in Figure 1 (Weller and Singer [1]), where some of the available experimental results for stringer stiffened shells are plotted as a function of Batdorf's Z ($= L^2/Rt\sqrt{1-\nu^2}$) parameter.

Trying to find the explanation of the wide experimental scatter and for the poor correlation between the predictions based on a linearized small deflection theory with SS-3 ($N_x = v = w = M_x = 0$) boundary conditions and the experimental values has occupied some of the most eminent scientists of this century. For thin shells that buckle elastically initial geometric imperfections (Koiter [2], Budiansky and Hutchinson [3]) and the effect of different boundary conditions (Hoff [4], Ohira [5], Singer and Rosen [6]) have been accepted as the main cause for the wide scatter of experimental results. However, this knowledge has not been, as yet, incorporated in the current shell design manuals.

These codes (Anonymous [7]) all adhere to the so-called "Lower Bound Design Philosophy" and as such recommend the use of the following buckling formula

$$P_a \leq \frac{\gamma}{F.S.} \cdot P_{CRIT} \qquad (1)$$

where P_a is the allowable applied load, P_{CRIT} is the lowest buckling load of the perfect structure, γ is a "knockdown factor" and F.S. is a factor of safety. The empirical knockdown factor γ is so chosen that when it is multiplied with P_{CRIT} a "lower bound" to all available experimental data is obtained.

It has been hoped that with the large scale introduction of advanced computer codes, which incorporate the latest theoretical findings, an alternative design procedure could be developed which would no longer penalize innovative shell design because of the poor experimental results obtained elsewhere. As a step towards this goal the results of an extensive numerical study with the well characterized stringer stiffened shell AS-2 tested at CALTECH in 1970 [8] are reported. The analysis is done with an early finite difference version of the well-known nonlinear shell code STAGS [9]. Discrete models of increasing size and complexity are employed in an attempt to reproduce numerically the experimentally observed shell behaviour.

2. COLLAPSE LOAD CALCULATIONS WITH STAGS

As stated in the introduction, with the 2-dimensional finite difference code STAGS one can calculate the effect of a given initial imperfection on the collapse load and at the same time enforce rigorously the experimental boundary conditions. However, the economical use of such programs requires not only some information about realistic imperfections that are present in the structure, but also considerable knowledge as to the physical behaviour of imperfect shell structures by the user. This knowledge can be acquired by first using the series of imperfection sensitivity analysis of increasing complexity which have been published in the open litterature in the past two decades.

The measured initial imperfection shape of the stringer stiffened shell AS-2 (see Fig. 2) is shown in Fig. 3 and its geometric and material properties are summarized in Table 1. Arbocz and Babcock published in 1980 a paper [10] wherein the results of the various imperfection sensitivity analysis applied to this particular shell were presented and compared to each other and to the test results. As can be seen from Table 2, with successive refinements in the model used the calculated buckling loads approach the experimental buckling load ever more. The STAGS (30-modes model) prediction of 243.8 N/cm is only about 7% off from the experimental value of 226.3 N/cm, a margin that is well within the accuracy that can be expected for imperfection sensitive buckling load calculations.

However, as has been pointed out in Reference 10 the recalculated initial imperfection shape using the 30 Fourier coefficients included in the analysis does not physically resemble the measured initial imperfection shape shown in Fig. 3. But since it describes so well the collapse behaviour of the shell AS-2 one could argue that the 30-modes model is equivalent (in some sense) to the actual initial shape. In the following it will be investigated what are the consequences of the different simplifying assumptions. Special attention will be devoted to the choice of the critical subsections of the complete shell structure, to the details of the imperfection models employed and to the satisfaction of the appropriate boundary conditions at the edges of the discrete models chosen.

2.1. Closed Model-Half the Shell Length

The shell segment used for the collapse analysis of the 30-modes imperfection model is shown in Fig. 4. The choice of the 40 x 40 mesh-size is dictated by the limits of computational facilities available in 1975 (a UNIVAC 1108). Because of the symmetry requirements at the boundaries 2 and 4 the 30-modes imperfection model [10] can only include cos nθ terms with n an even integer. This restriction means that the imperfection representation used is symmetric with respect to θ = 0. An assumption that does not agree with the measured initial imperfection shown in Fig. 3.

In order to remove this restriction initially the shell segment shown in Fig. 5 is used. The chosen meshsize of 19 x 221 represents the limit of the computational facilities available in Delft (an AMDAHL 470-V7B). To represent the measured imperfections initially the following double Fourier series is used:

$$\bar{w}(x,y) = t \sum A_{io} \cos \frac{i\pi x}{L} + t \sum A_{o\ell} \cos \frac{\ell y}{R} + t \sum B_{o\ell} \sin \frac{\ell y}{R}$$

$$+ \sum\sum \sin \frac{k\pi x}{L} \left(C_{k\ell} \cos \frac{\ell y}{R} + D_{k\ell} \sin \frac{\ell y}{R}\right) \qquad (2)$$

By the selection of the initial imperfection harmonics to be included in the analysis first all those harmonics are taken the amplitudes of which are greater than 0.040 (4% of the wall thickness t) and which satisfy the symmetry condition with respect to x = L/2. Next the required "breathing-like" modes, which satisfy the condition i = 2k are added. Finally one selects the coupling modes that must be included in order to satisfy the coupling conditions $k_1 + k_2 + k_3$ = odd integer and $|\ell_1 \pm \ell_2| = \ell_3$. For the present case these conditions resulted in the 74-modes imperfection model summarized in Table 3. Notice that the amplitudes of the higher order buckling modes are set equal to 0.005 (0,5% of the wall thickness t).

The recomputed initial shape of the 74-modes initial imperfection model is shown in Fig. 6. It includes both cos nθ and sin nθ terms and satisfies the symmetry conditions at x = L/2 (boundary 3) as required by the shell segment shown in Fig. 5. Figure 7 displays the determination of the limit point, where close to the collapse load ρ_s = 0.8026 very small load increments had to be used. The normalized collapse load is defined as follows: $\rho_s = N_x/(-320.8)$ where -320.8 N/cm is the buckling load of the perfect shell AS-2 using membrane prebuckling and C4- ($u = v = w = w_{,x} = 0$) boundary conditions. Figure 8 shows the calculated prebuckling deformation and Fig. 9 the collapse mode at the limit loads ρ_s = 0.8026. As indicated in Fig. 9 the collapse mode represents the difference of the last two prebuckling solutions and it consists of a single buckle in the central region of the shell. This agrees with the published high speed movies of the buckling process obtained by Almroth [11] and Esslinger [12].

Next as an alternate representation the lower-half of the measured initial data is fitted by a bivariate cubic spline fit which, as can be seen from Fig. 10, smoothens rather nicely the original experimental data recorded at a rather coarse 21 x 49 mesh. The bivariate cubic spline fitted model is then used to compute the first derivatives with respect to x and θ of the measured initial imperfection at all nodal points of the 19 x 221 mesh. This data is then read in directly by STAGS via a user written subroutine. Unfortunately this imperfection model does not satisfy rigorously the symmetry conditions at x = L/2 which are imposed by the shell segment used for this analysis (see Fig. 5). Thus the collapse load is ρ_s = 0.8451 (once again normalized by -320.8 N/cm), a higher value then the one found for the 74-modes imperfection model. However, the calculated prebuckling deformation shown in Fig. 11 and the collapse mode displayed in Fig. 12 are nearly identical to the ones obtained previously (compare with Figures 8 and 9, respectively).

Spline fitting, in turn, the upper-half of the measured initial imperfection data results in the pattern shown in Fig. 13. This bivariate cubic spline fitted model is then used to compute the first derivatives with respect to x and θ of the measured initial imperfection data at all nodal points of the upper 19 x 221 mesh, which then are read in directly by STAGS via a user written subroutine. One again the fitted imperfection model does not satisfy the symmetry conditions at x = L/2. Thus the collapse load is ρ_s = 0.84101 (normalized by -320.8 N/cm), somewhat lower than the value obtained using the spline fitted lower-half model but still higher than the value found for the 74-modes imperfection model. The calculated prebuckling deformation pattern shown in Fig. 14 and the collapse model displayed in Fig. 15 are very similar to the corresponding figures obtained using the spline fitted lower-half model (compare with Figures 11 and 12, respectively).

2.2. Open Model-Half the Shell Perimeter

It is known that the lowest buckling mode of the perfect stringer stiffened

shell AS-2 is asymmetric in the axial direction [13]. Thus by choosing the discrete model shown in Fig. 16, where the full shell length is modeled, these asymmetric modes can develop unimpeded. Further by using half the shell perimeter ($\Delta\theta = 180^o$) it is hoped that the effect of the boundary conditions at $\theta = 0$ and $\theta = 180^o$ can be minimized.

Initially the measured initial imperfections are represented by the double Fourier series (see Eq. (2)) used previously. When selecting the initial imperfection harmonics to be included in the analysis first all those harmonics are taken the amplitudes of which are greater than 0.040. Notice that the symmetry restriction with respect to $x = L/2$ is no longer applicable. Next the "breathing-like" modes, which satisfy the condition $i = 2k$ are added. Finally the coupling modes (defined as those modes which are needed in order to satisfy the coupling conditions $k_1 + k_2 + k_3 =$ odd integer and $|\ell_1 \pm \ell_2| = \ell_3$) are included. These conditions resulted in the 132-modes imperfection model summarized in Table 4. Notice that the amplitudes of the higher order coupling modes are once again equal to 0.005 (0.5% of the wall thickness t). The recomputed initial shape of the 132-modes initial imperfection model shown in Fig. 17 resembles rather well to the measured initial imperfection shown in Fig. 3. However, since both $\sin n\theta$ and $\cos n\theta$ components are included, it only partially satisfies the symmetry conditions at $\theta = 0$ and $\theta = 180^o$ (at boundaries 2 and 4) imposed by the discrete model used. The chosen mesh of 61 x 161 has been based on the results of convergence studies reported in Reference 13. The collapse load is $\rho_s = 0.78619$ (normalized by -320.8 N/cm). Thus not satisfying rigorously the symmetry conditions in the circumferential direction (at $\theta = 0$ and $\theta = 180^o$) seems to have less stiffening effect then the not satisfying of the symmetry conditions at $x = L/2$. The calculated prebuckling deformation shown in Fig. 18 and the collapse mode at the limit point $\rho_s = 0.78619$ displayed in Fig. 19 are very similar to the corresponding deformation patterns obtained previously (compare with Figures 8, 9 and 11 and 12 respectively).

Switching to the bivariate cubic pline fit, initially the left-half of the shell perimeter is fitted, whereby first a switch of the circumferential origin $\theta = 0$ is executed so that the region of the expected maximum response is placed at the central part of the shell segment. Figure 20 shows the spline fitted initial imperfection surface used for the collapse load calculations. It can be seen clearly that at the edges $\theta = 0$ and $\theta = 180^o$ the symmetry conditions are not satisfied. Thus it comes as no suprise that the limit load is $\rho_s = 0.8727$ (normalized by -320.8 N/cm), a rather high value. On the other hand the calculated prebuckling deformation and the collapse mode at $\rho_s = 0.8727$ shown in Figures 21 and 22 do not differ much from the corresponding plots obtained previously.

The next case is an excellent example of what can happen if one just "blindly" chooses a shell segment around the location where the maximum initial radial imperfection is located, without performing the necessary preliminary analysis so as to acquire sufficient information about the expected behaviour of the sample shell. Figure 23 shows the spline fitted initial imperfection of the "shifted" right-half of the shell AS-2. Notice that the origin $\theta = 0$ is shifted so that the maximum initial radial imperfection is placed at about the central part of the shell segment used. The normalized collapse load is here $\rho_s = 0.9513$ (with the same normalization factor of -320.8 N/cm). Looking at the calculated prebuckling deformation at $\rho_s = 0.9513$ shown in Fig. 24 it is immediately evident that it is completely different from the other prebuckling shapes obtained sofar. Comparing it to the bifurcation buckling mode of the perfect stringer stiffened shell AS-2 with the same C-4 ($u = v = w = w_{,x} = 0$) boundary conditions shown in Fig. 25, it is clear that in this case the form of the initial imperfection used has a stabilizing effect and that the shell segment collapses only when about the perfect shell buckling load is reached. This statement is reinforced further by the collapse mode at $\rho_s = 0.9513$ displayed in Fig. 26, which resembles very closely the bifurcation buckling mode of the perfect shell shown in Fig. 25.

2.3. Closed Model-Complete Shell

From the results obtained sofar it is clear that the value of the collapse load ρ_s is strongly influenced by the well or not satisfaction of the symmetry conditions at the edges of the shell sub-sections used in the collapse analysis. One way of avoiding these problems is by modeling the complete shell. However, as can be seen from Fig. 27, the use of a closed shell model requires displacement continuity at the boundaries 2 and 4, which results in rather large band width thus increasing the execution times considerably. Notice that the spline fitted initial imperfection surface shown in Fig. 28 agrees quite well with the measured initial imperfection of Fig. 3. The mesh of 41 x 161 used for the collapse load calculation with the closed shell model represents just about the limit of what can be computed on the currently available Amdahl 470-V7B in Delft. The calculated prebuckling deformation at the limit point $\rho_s = 0.8563$ is displayed in Fig. 29, the corresponding collapse mode is shown in Fig. 30. The agreement with the previously calculated deformation patterns is reasonably good, however, the collapse load of $\rho_s = 0.8563$ (normalized by -320.8 N/cm) is unexpectedly high.

In looking for an explanation, a comparison of the calculated prebuckling pattern of Fig. 29 with the experimentally measured prebuckling deformation of Fig. 31 is helpful. It is obvious that the two deformation patterns are strikingly different. Since the measured initial imperfections are modelled quite accurately by the bivariate cubic spline fit used, therefore the answer must be sought in a possible difference between the C-4 ($u = v = w = w_{,x} = 0$) boundary conditions used with the numerical calculations and the actual boundary conditions present at the experimental set-up.

In Reference 13 the effect of boundary conditions on the bifurcation buckling load of the perfect stringer stiffened shell AS-2 has been extensively investigated. The conclusion was that the two end-pieces used in the experimental set-up appeared stiff enough to simulate the C-4 ($u = v = w = w_{,x} = 0$) boundary conditions. It seems, however, that this conclusion arrived at in Reference 13 by using perfect shell analysis does not hold for shells with initial imperfections. This statement is reinforced by the result of rerunning the current model using the same spline fitted inital imperfections as input but changing the boundary conditions successively to C-3 ($N_x = v = w = w_{,x} = 0$) and to SS-3 ($N_x = v = w = M_x = 0$). The calculated prebuckling deformations are shown in Figures 32 and 33, respectively. It must be mentioned here that for the C-3 boundary conditions the limit load $\rho_s = 0.8153$ is normalized by -256.9 N/cm; whereas for the SS-3 boundary conditions the limit load $\rho_s = 0.8095$ is normalized by -229.8 N/cm. The normalizing factors are the bifurcation buckling loads of the perfect stringer stiffened shell AS-2 using membrane prebuckling and the indicated boundary conditions.

From a comparisom of Figures 29, 32 and 33 (displaying the calculated prebuckling deformations using the different boundary conditions as indicated) with the measured prebuckling growth shown in Fig. 31 it is clear that the best agreement occurs for the SS-33 boundary conditions. Thus it appears that in order to model the buckling behaviour of the imperfect stringer stiffened shell AS-2 accurately one must not only include the measured initial imperfections but also model the experimental boundary conditions more realistically. This means that one must use the appropriate elastic boundary conditions in place of the standard, mathematically so convenient C-4, SS-3 etc. boundary conditions.

3. DISCUSSION OF THE NUMERICAL RESULTS

As has been reported in Reference 8, because of clearence problems with the head of the capacitance pick-up the circumferential scans had to be started and stopped at about 0,9 cm from the shell ends. Thus two narrow regions next to the shell edges remained unscanned. In Figures 3 and 31, which display the measured initial imperfections and the measured prebuckling deformation at $\rho = 0.629$, these regions are represented by the parallel lines next to the lower ($x = 0$) and the upper ($x = 139.7$ mm) shell edges. The harmonic analysis is done based on this reduced length. For the buckling load calculations, however, the real physical length of the shell is used, whereby one assumes that the contribution of the imperfections within the (neglected) narrow edge regions to the harmonic content of the surface scans is negligible. For the cubic spline fitted imperfections extrapolation is employed to obtain the needed imperfection data in the narrow unscanned boundary regions.

The determination of limit points, as is done in Fig. 7, by looking for that load level beyond which the nonlinear iterative solution fails to converge is somewhat unsatisfactory. Close to the limit point it requires the use of very small incremental quantities and solutions beyond the limit point are very difficult to obtain. Recently Riks' solution procedure [14] has been incorporated in the STAGS-A program used in Delft. Check runs with this new version of the code, which can obtain converged solutions beyond the limit point routinely, have confirmed the axial load levels at the limit points found earlier.

A detailed convergence study with the STAGS-A code [10], based on bifurcation buckling of the perfect AS-2 shell, indicates the need for a 41 x 241 mesh if a complete shell is employed for the collapse analysis. Such a model is as yet beyond the available computational facilities. The results of a limited convergence study with the imperfect AS-2 shell, using 41 rows and 141, 161 and 181 columns respectively, are shown in Fig. 34. Here along the vertical axis the percent change in axial load as referred to the preceding model is plotted. As can be seen the 3 points obtained seem to confirm the predictions of the earlier convergence study from Reference 10.

General information about the computer runs described in this paper are presented in Table 5. With the exception of the 30 modes imperfection model which was run on an UNIVAC 1108, all other runs were executed on the AMDAHL 470-V7B in Delft. Initially one refactoring of the stiffness matrix per restart is sufficient. Close to the limit point refactoring at every load step may be required. Due to extensive use of secondary storage the ELAPSED times needed exceed the CPU times used by about a factor of 3. Thus most runs are executed during the weekends in the "UNATTENDED" mode.

4. CONCLUSIONS

The results of this study show that by combining the existing nonlinear analysis capabilities with detailed knowledge of the expected shell behaviour, one indeed can find relatively small discrete models consisting of subsections of the complete shell which will adequately predict the actual collapse load.

Thus the 30-modes imperfection model does a good prediction of the experimental collapse load because it models the rather localized collapse mechanism of the stringer stiffened shell AS-2 satisfactorily. On the other hand, the use of the cubic spline fitted imperfection model to that part of the shell where the maximum radial imperfection is located triggered only the overall collapse mechanism of the perfect shell. The predicted collapse load was thus much higher than the experimental value.

In general the proper double Fourier series representation of the initial imperfections will lead to a close prediction of the experimental collapse load, if the appropriate symmetry conditions at the edges of the shell subsection used for the analysis are satified. Since the cubic spline fitted imperfection description in general does not satisfy the required symmetry conditions its use with shell subsections is not recommended.

Finally, the runs with identical imperfections but different boundary conditions clearly indicate that the form of the resulting prebuckling deformation is strongly influenced by the interaction between initial imperfections and the different types of boundary constraints present. Thus the results of this paper support the contention of Singer and Rosen [6], that for the stringer stiffened shells a better correlation between theoretical predictions and experimental results requires the inclusion of both the initial imperfections and the appropriate elastic boundary conditions in the analysis.

5. REFERENCES

1. Weller, T. & Singer, J.: "Recent Experimental Studies on the Buckling of Integrally Stringer-Stiffened Shells", TAE Report No. 100, Technion-Israel Institute of Technology, Department of Aeronautical Engineering, Haifa, Israel, 1970.

2. Koiter, W.T.: "On the Stability of Elastic Equilibrium", Ph.D. Thesis, in Dutch, TH Delft, Netherlands, H.T. Paris, Amsterdam, 1945 (English translation issued as NASA TT F-10, 1967).

3. Budiansky, B. & Hutchinson, J.W.: "Dynamic Buckling of Imperfection Sensitive Structures", In: Proceedings 11th IUTAM Congress, Springer Verlag Berlin, pp. 636-51, 1964.

4. Hoff, N.J.: "Buckling of Thin Shells", In: Proceedings of an Aerospace Symposium of Distinguished Lecturers in Honor of Theodore von Kármán on his 80th Anniversary, Institute of Aerospace Sciences, New York, pp. 1-42, 1961.

5. Ohira, H.: "Local Buckling Theory of Axially Compressed Cylindrical Shells", In: Proceedings 11th Japan National Congress of Applied Mechanics", pp. 37-40, 1961.

6. Singer, J. & Rosen, A.: "The Influence of Boundary Conditions on the Buckling of Stiffened Cylindrical Shells", In: Proceedings IUTAM Symposium Buckling of Structures, Harvard University, Cambridge, Mass., June 1974, B. Budiansky (ed.), Springer Verlag Berlin, pp. 227-50, 1976.

7. Anonymous: "Buckling of Thin-Walled Cylinders", NASA Space Vehicle Design Criteria (Structures), NASA SP-8007, revised, 1968.

8. Singer, J., Arbocz, J. & Babcock, C.D. Jr.: "Buckling of Imperfect Stiffened Cylindrical Shells under Axial Compression", AIAA Journal, Vol. 9, No. 1, pp. 68-75, Jan. 1971.

9. Almroth, B.O., Brogan, F.A., Miller, E., Zele, F. & Peterson, H.T.: "Collapse Analysis for Shells of General Shape". II User's Manual for the STAGS-A Computer Code, Air Force Flight Dynamic Lab., Wright-Patterson AFB, AFFDL-TR-71-8, 1973.

10. Arbocz, J. & Babcock, C.D. Jr.: "The Buckling Analysis of Imperfection Sensitive Shell Structures", NASA CR-3310, August 1980.

11. Almroth, B.O., Holmes, A.M.C. and Brush, D.O.: "An Experimental Study of the Buckling of Cylinders under Axial Compression", Report 6-90-63-104, Lockheed Missiles and Space Company, Palo Alto, California, 1963.

12. Esslinger, M.: "Hochgeschwindigkeitsaufnahmen vom Beulvorgang dünnwandiger, axialbelasteter Zylinder", der Stahlbau, Vol. 39, No. 3, pp. 73-76, 1970.

13. Arbocz, J. & Babcock, C.D. Jr.: "Utilization of STAGS to Determine Knockdown Factors from Measured Initial Imperfections", Report LR-275, Department of Aerospace Engineering, TH Delft, The Netherlands, Nov. 1978.

14. Riks, E.: "Development of an improved analysis capability of the STAGS computer code with respect to the collapse behaviour of shell structures", Memorandum SC-79-059, National Aerospace Laboratory NLR, The Netherlands, 1979.

Table 1. Geometric and material properties of shell AS-2

t	$= 1.96596 \times 10^{-2}$ cm	(= 0.00774	IN)
L	$= 13.97$ cm	(= 5.5	IN)
R	$= 10.16$ cm	(= 4.0	IN)
d_1	$= 8.03402 \times 10^{-1}$ cm	(= 0.3163	IN)
e_1	$= 3.36804 \times 10^{-2}$ cm	(= 0.01326	IN)
A_1	$= 7.98708 \times 10^{-3}$ cm^2	(= 0.1238×10^{-2}	IN^2)
I_{11}	$= 1.50384 \times 10^{-6}$ cm^4	(= 0.3613×10^{-7}	IN^4)
I_{t1}	$= 4.94483 \times 10^{-6}$ cm^4	(= 0.1188×10^{-6}	IN^4)
E	$= 6.89472 \times 10^{6}$ N/cm^2	(= 10.10^6	PSI)
ν	$= 0.3$		

Table 2. Summary of buckling load calculations

Conditions	Loads (N/cm)
Perfect shell analysis	
Experimental set-up	316.6
Fully clamped - Nonlinear bending prebuckling	316.8
Fully clamped - Membrane prebuckling	320.8
Simply supported Membrane prebuckling	229.8
Imperfect shell analysis	
Koiter type (b-factor)	295.1
Multi mode analysis (7-modes model)	264.7
STAGS (30-modes model)	243.8
Experimental buckling load	226.3

Table 3. The 74-modes imperfection model ($\bar{w}$ is positive outward)

Harmonics with amplitudes greater than 0.040

Mode no.	k	ℓ	$A_{k\ell}$	Mode no.	k	ℓ	$B_{k\ell}$
1	0	2	0.246	5	0	2	0.094
2	0	3	0.165	6	0	6	-0.070
3	0	4	0.179				
4	0	9	0.058				
			$D_{k\ell}$				$D_{k\ell}$
7	1	2	0.315	19	1	2	0.118
8	1	3	0.208	20	1	5	0.046
9	1	4	0.231	21	1	6	-0.093
10	1	7	0.041	22	1	10	0.041
11	1	8	-0.066	23	1	11	-0.055
12	1	9	0.081	24	3	2	0.040
13	3	2	0.100				
14	3	3	0.072				
15	3	4	0.071				
16	5	2	0.058				
17	5	3	0.041				
18	5	4	0.040				

"Breathing-like" modes

Mode no.	k	ℓ	$A_{k\ell}$
25	2	0	0.0046
26	4	0	0.0036
27	6	0	-0.0003
28	8	0	-0.0020
29	10	0	-0.0014

Coupling modes with measured amplitudes

Mode no.	k	ℓ	$C_{k\ell}$	Mode no.	k	ℓ	$D_{k\ell}$
30	1	5	-0.020	42	1	3	-0.029
31	1	6	-0.037	43	1	4	-0.006
32	1	10	-0.037	44	1	7	-0.038
33	1	11	0.003	45	1	8	-0.001
34	1	12	0.038	46	1	9	-0.037

Coupling modes with measured amplitudes

Mode no.	k	ℓ	$C_{k\ell}$	Mode no.	k	ℓ	$D_{k\ell}$
35	1	13	-0.031	47	1	12	0.027
36	1	14	0.033	48	1	13	0.002
37	1	15	-0.002	49	1	14	-0.014
38	1	16	-0.007	50	1	15	0.029
39	1	17	0.016	51	1	16	-0.020
40	1	18	-0.018	52	1	17	-0.002
41	1	19	0.008	53	1	18	-0.003
				54	1	19	-0.008

Coupling modes with amplitudes of 0.005

$C_{1,21}$, $C_{1,23}$, $C_{1,24}$, $C_{1,25}$, $C_{1,27}$, $C_{1,29}$, $C_{1,31}$

$C_{1,33}$, $C_{1,35}$, $C_{1,37}$

$D_{1,21}$, $D_{1,23}$, $D_{1,24}$, $D_{1,25}$, $D_{1,27}$, $D_{1,29}$, $D_{1,31}$

$D_{1,33}$, $D_{1,35}$, $D_{1,37}$

Table 4. The 132-modes imperfection modes ($\bar{w}$ is positive outward)

Harmonics with amplitudes greater than 0.040

Mode no.	k	ℓ	$A_{k\ell}$	Mode no.	k	ℓ	$B_{k\ell}$
1	0	2	0.246	5	0	2	0.094
2	0	3	0.165	6	0	6	-0.070
3	0	4	0.179				
4	0	9	0.058				
			$C_{k\ell}$				$D_{k\ell}$
7	1	2	0.315	21	1	2	0.118
8	1	3	0.208	22	1	5	0.046
9	1	4	0.231	23	1	6	-0.093
10	1	7	0.041	24	1	10	0.041
11	1	8	-0.066	25	1	11	-0.055
12	1	9	0.081	26	2	2	-0.072
13	2	2	0.198	27	2	3	-0.073
14	2	4	0.057	28	3	2	0.040
15	3	2	0.100				
16	3	3	0.072				
17	3	4	0.071				
18	5	2	0.058				
19	5	3	0.041				
20	5	4	0.040				

"Breathing-like" modes

Mode no.	k	ℓ	$A_{k\ell}$
29	2	0	0.0046
30	4	0	0.0036
31	6	0	-0.0003
32	8	0	-0.0020
33	10	0	-0.0014

Coupling modes with measured amplitudes

Mode no.	k	ℓ	$C_{k\ell}$	Mode no.	k	ℓ	$D_{k\ell}$
34	1	5	-0.020	63	1	3	-0.029
35	1	6	-0.037	64	1	4	-0.006
36	1	10	-0.037	65	1	7	-0.038
37	1	11	0.003	66	1	8	-0.001
38	1	12	0.038	67	1	9	-0.037
39	1	13	-0.031	68	1	12	0.027
40	1	14	0.033	69	1	13	0.002
41	1	15	-0.002	70	1	14	-0.014
42	1	16	-0.007	71	1	15	0.029
43	1	17	0.016	72	1	16	-0.020
44	1	18	-0.018	73	1	17	-0.002
45	1	19	0.008	74	1	18	-0.003
46	2	3	-0.012	75	1	19	-0.008
47	2	5	-0.015	76	2	4	0.005
48	2	6	-0.010	77	2	5	-0.013
49	2	7	-0.018	78	2	6	-0.004
50	2	8	-0.012	79	2	7	-0.012
51	2	9	0.001	80	2	8	-0.002
52	2	10	-0.018	81	2	9	0.0002
53	2	11	-0.001	82	2	10	0.009
54	2	12	-0.006	83	2	11	-0.006
55	2	13	-0.002	84	2	12	0.002
56	2	14	0.002	85	2	13	0.001
57	2	15	-0.004	86	2	14	-0.001
58	2	16	-0.001	87	2	15	0.0002
59	2	17	0.002	88	2	16	0.001
60	2	18	-0.0003	89	2	17	0.003
61	2	19	0.002	90	2	18	0.003
62	2	20	-0.0001	91	2	19	-0.001
				92	2	20	0.0001

Coupling modes with amplitudes of 0.005

$C_{1,21}$, $C_{1,23}$, $C_{1,24}$, $C_{1,25}$, $C_{1,27}$, $C_{1,29}$, $C_{1,31}$, $C_{1,33}$, $C_{1,35}$, $C_{1,37}$
$C_{2,22}$, $C_{2,24}$, $C_{2,26}$, $C_{2,28}$, $C_{2,30}$, $C_{2,32}$, $C_{2,34}$, $C_{2,36}$, $C_{2,38}$, $C_{2,40}$
$D_{1,21}$, $D_{1,23}$, $D_{1,24}$, $D_{1,25}$, $D_{1,27}$, $D_{1,29}$, $D_{1,31}$, $D_{1,33}$, $D_{1,35}$, $D_{1,37}$
$D_{2,22}$, $D_{2,24}$, $D_{2,26}$, $D_{2,28}$, $D_{2,30}$, $D_{2,32}$, $D_{2,34}$, $D_{2,36}$, $D_{2,38}$, $D_{2,40}$

Table 5. General information about the runs presented

Shell segment	Imperfection model	Mesh	Unknowns	Max. band width	Load steps	Restarts	Factoring (hrs)	CPU time (hrs)
Fig. 4	30 modes	40x40	5120	332	8	6	0.6	7.0
Fig. 5	74 modes	19x221	14049	1994	35	8	7.3	123,5
Fig. 5	Cubic spline (lower half)	19x221	14049	1994	35	3	7.3	48.6
Fig. 5	Cubic spline (upper half)	19x221	14049	1994	29	4	7.3	112.2
Fig. 16	132 modes	61x161	30807	384	26	6	1.3	19.2
Fig. 16	Cubic spline (left half)	61x161	30807	384	20	5	1.3	23.0
Fig. 16	Cubic spline (right half)	61x161	30807	384	32	7	1.3	24.7
Fig. 27	Cubic spline (C-4)	41x161	21027	1454	22	5	5.8	55.5
Fig. 27	Cubic spline (C-3)	41x161	21027	1454	32	6	5.8	72.2
Fig. 27	Cubic spline (SS-3)	41x161	21027	1454	31	5	5.8	52.6

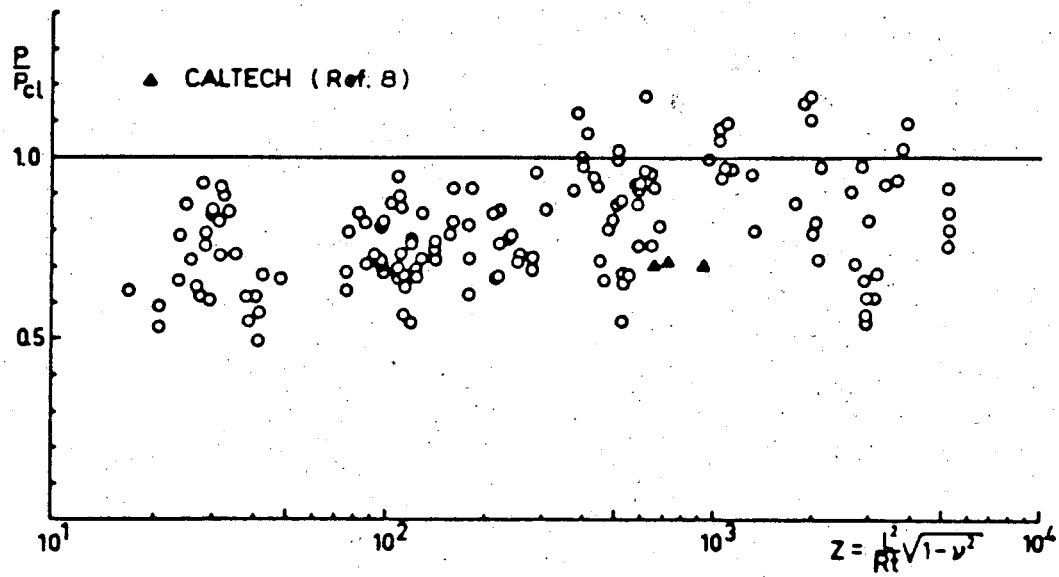

Fig. 1 Comparison of theory and experiment for stringer stiffened shells under axial compression [1]

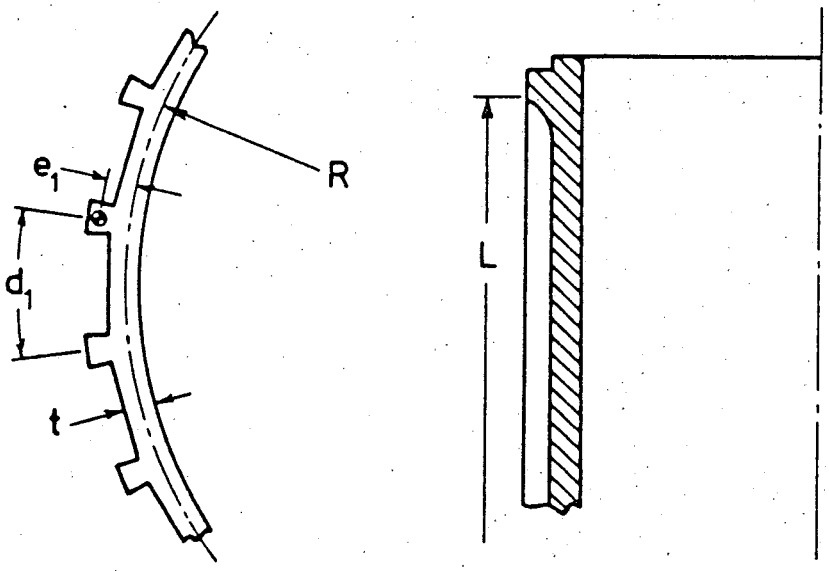

Fig. 2 Geometry of the stringer stiffened shell AS-2 [8]

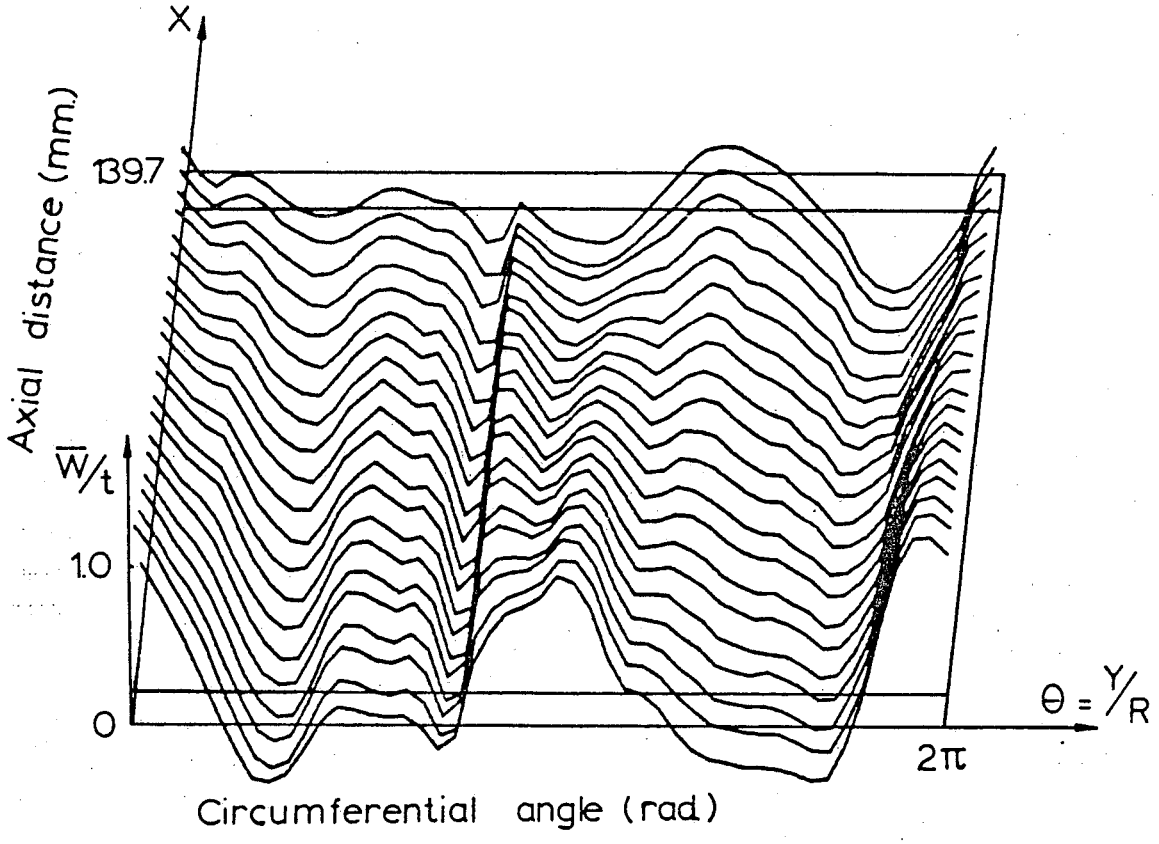

Fig.3 Measured initial shape of the stringer stiffened shell AS-2 (21 x 49 = 1029 data points)

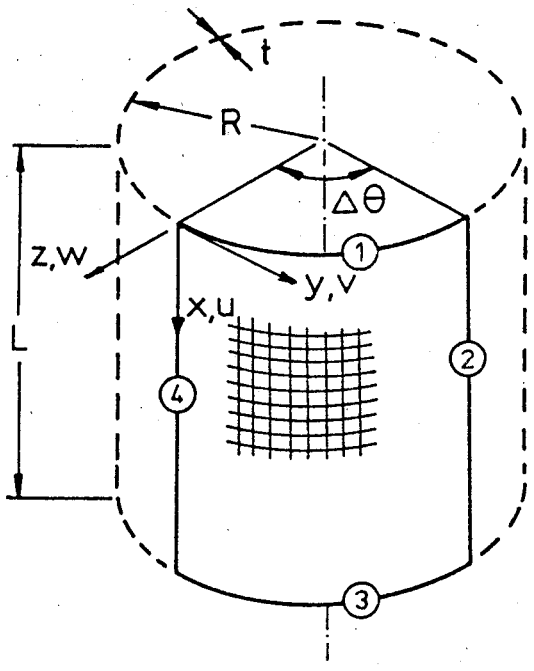

Boundary conditions

① $u \neq 0$, $v = w = w_{,x} = 0$

②, ④ symmetry

③ $u = v = w = w_{,x} = 0$

$\Delta\theta = 90°$

Fig. 4 Shell segment used for collapse analysis of imperfect shells (Discrete model A)

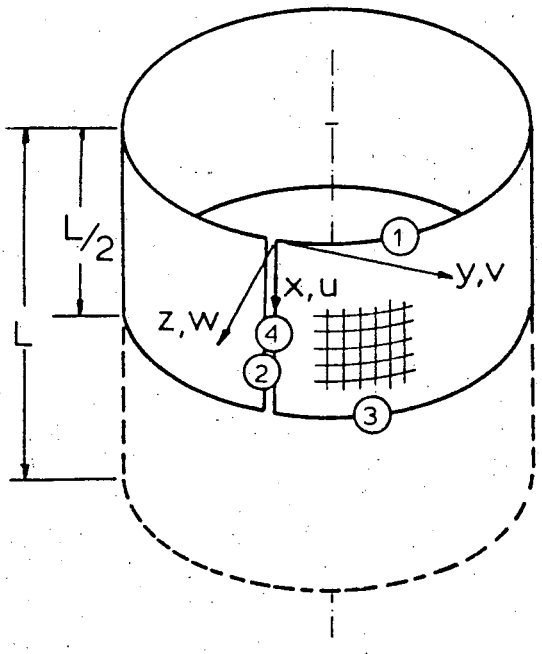

Boundary conditions

① $u \neq 0$, $v = w = w_{,x} = 0$

②,④ displacement compatibility

③ symmetry

$\Delta\theta = 360°$

Fig. 5 Shell segment used for collapse analysis of imperfect shells (Discrete model B)

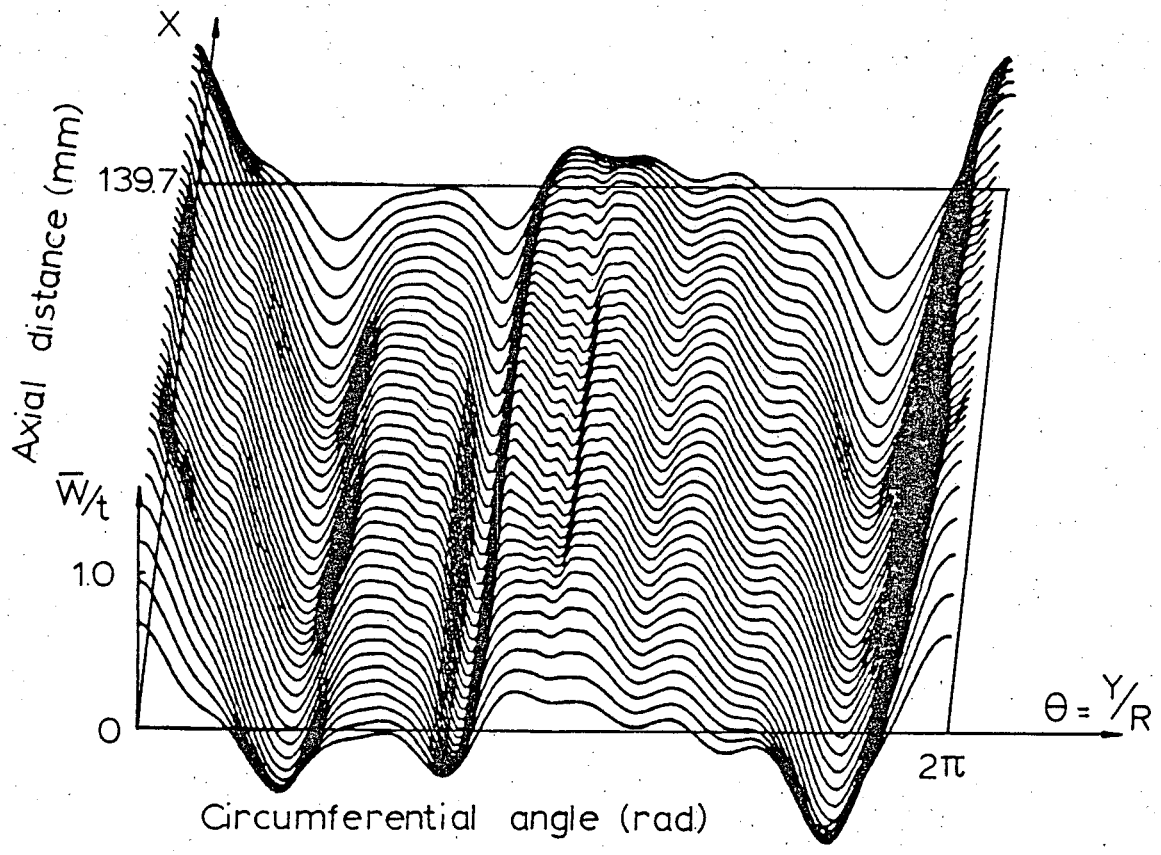

Fig. 6 Recomputed initial shape of the stringer stiffened shell AS-2 using 74 Fourier coefficients

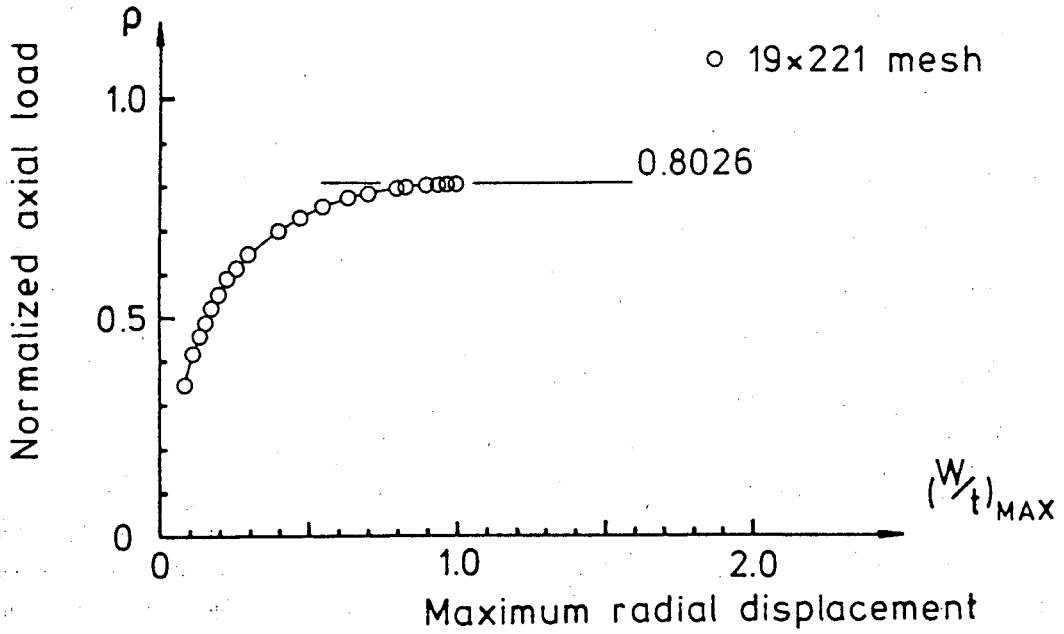

Fig. 7 Determination of the limit point by STAGS analysis (Shell AS-2, Boundary conditions: $u=v=w=w_{,x}=0$)

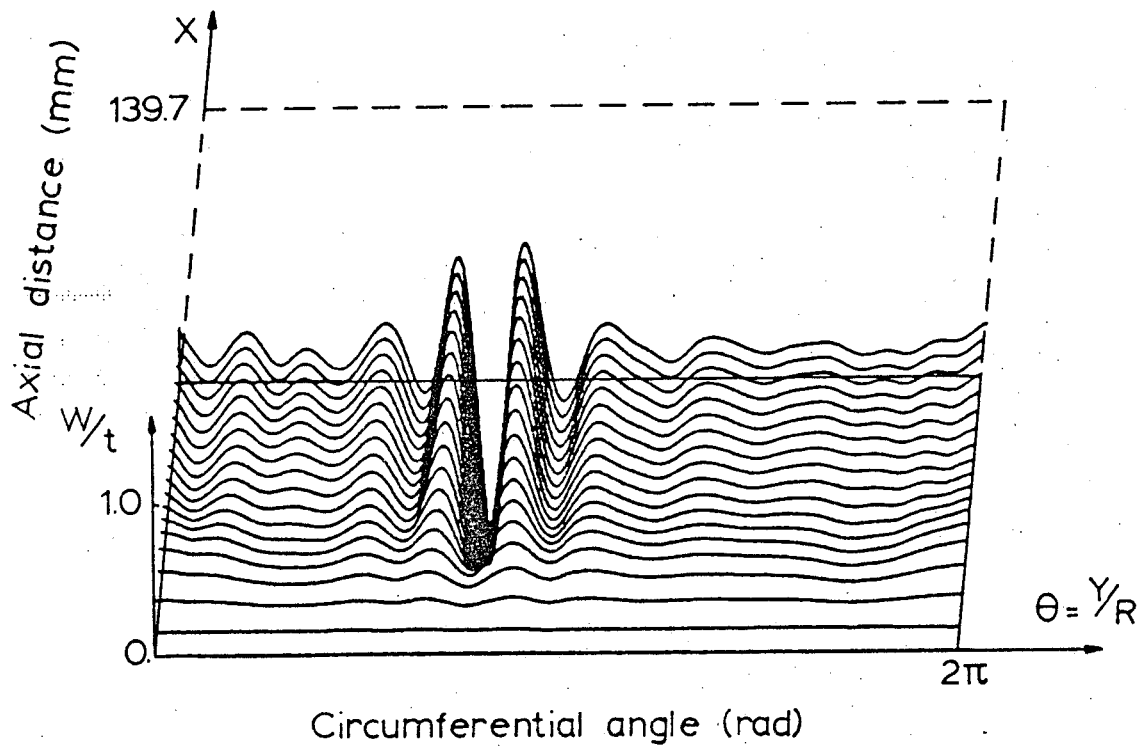

Fig. 8 Calculated prebuckling growth of the stringer stiffened shell AS-2 at $\rho_s=0.8026$ (19 x 221 = 4199 mesh points) (Boundary conditions: $u=v=w=w_{,x}=0$)

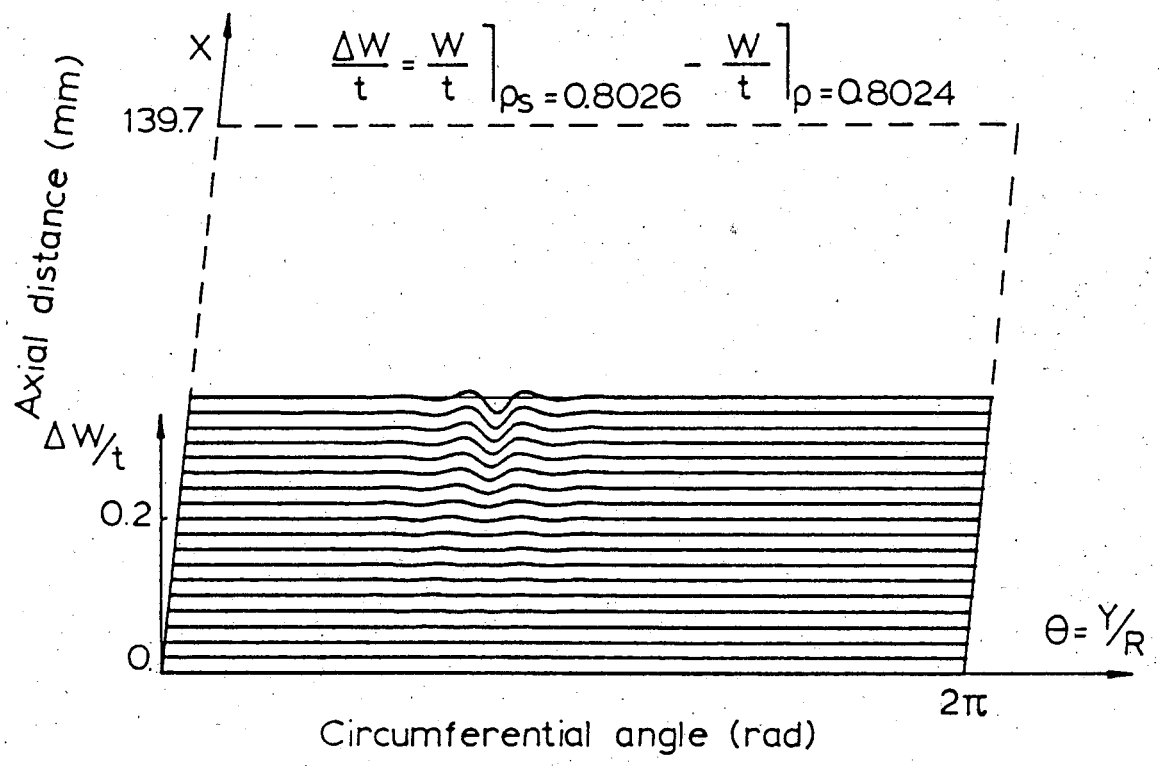

Fig.9 Calculated collapse mode of the stringer stiffened shell AS-2 at $\rho_s = 0.8026$ (19 x 221 = 4199 mesh points) (Boundary conditions: $u=v=w=w_{,x}=0$)

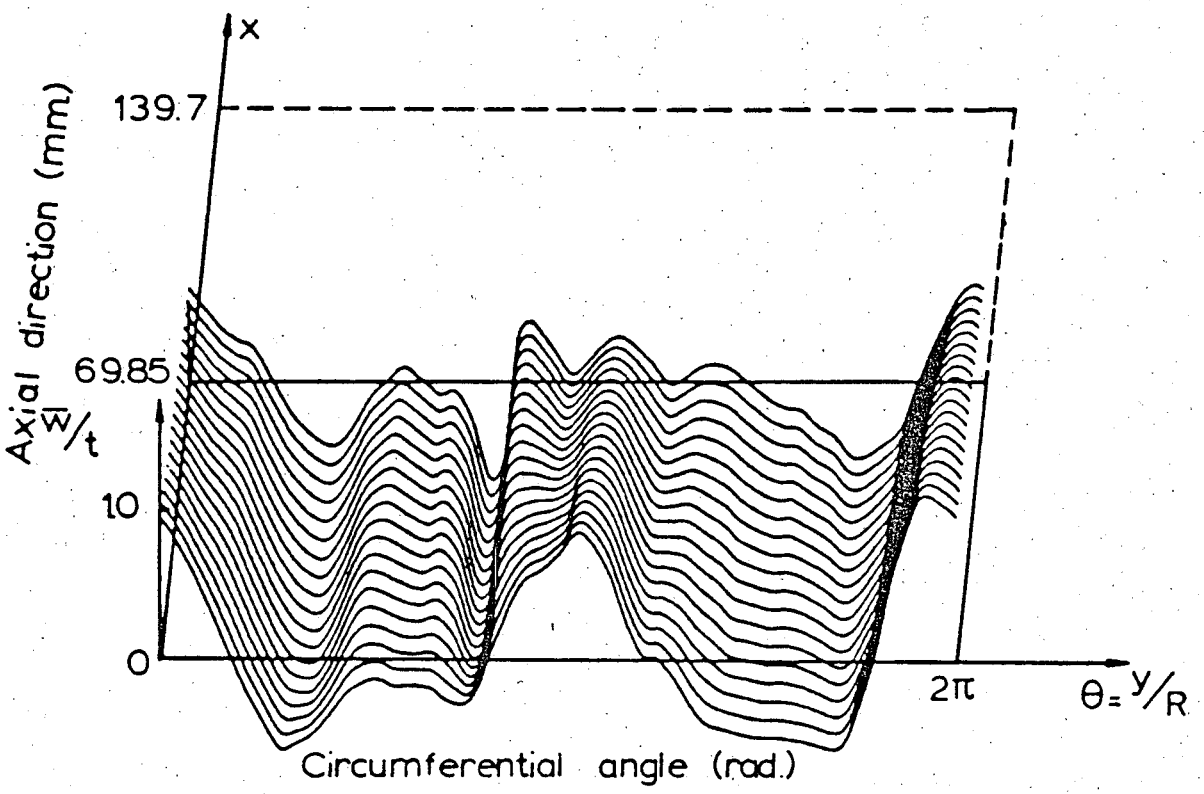

Fig. 10 Cubic spline fitted initial shape of the stringer stiffened shell AS-2 (19 x 221 = 4199 mesh points)

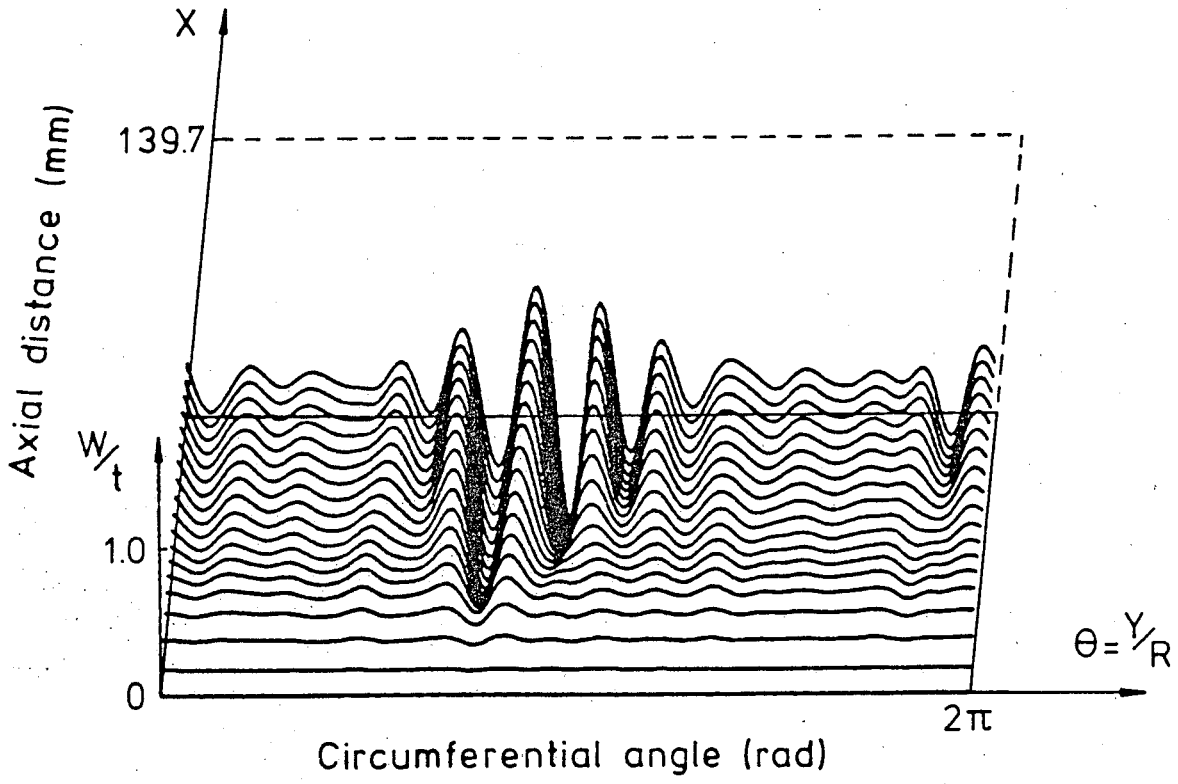

Fig.11 Calculated prebuckling growth of the stringer stiffened shell AS-2 at ρ_s=0.8451 (19×221 mesh points) (Boundary conditions: $u=v=w=w_{,x}=0$)

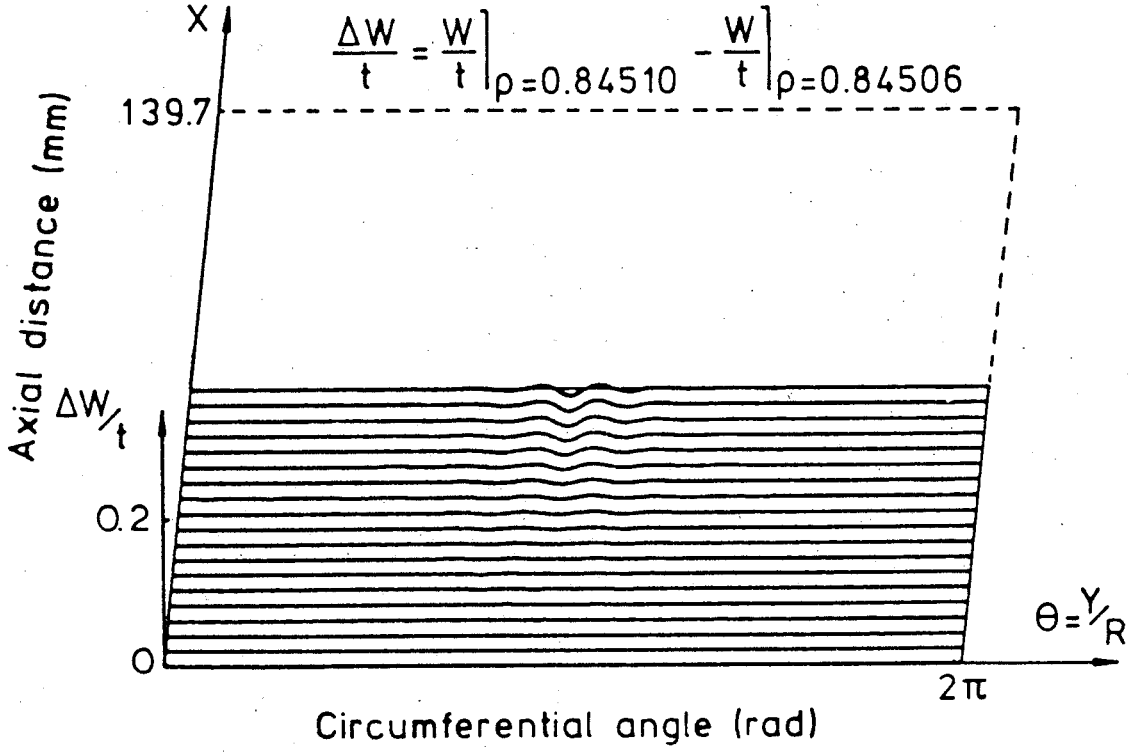

Fig.12 Calculated collapse mode of the stringer stiffened shell AS-2 at ρ_s=0.8451 (19×221 mesh points) (Boundary conditions: $u=v=w=w_{,x}=0$)

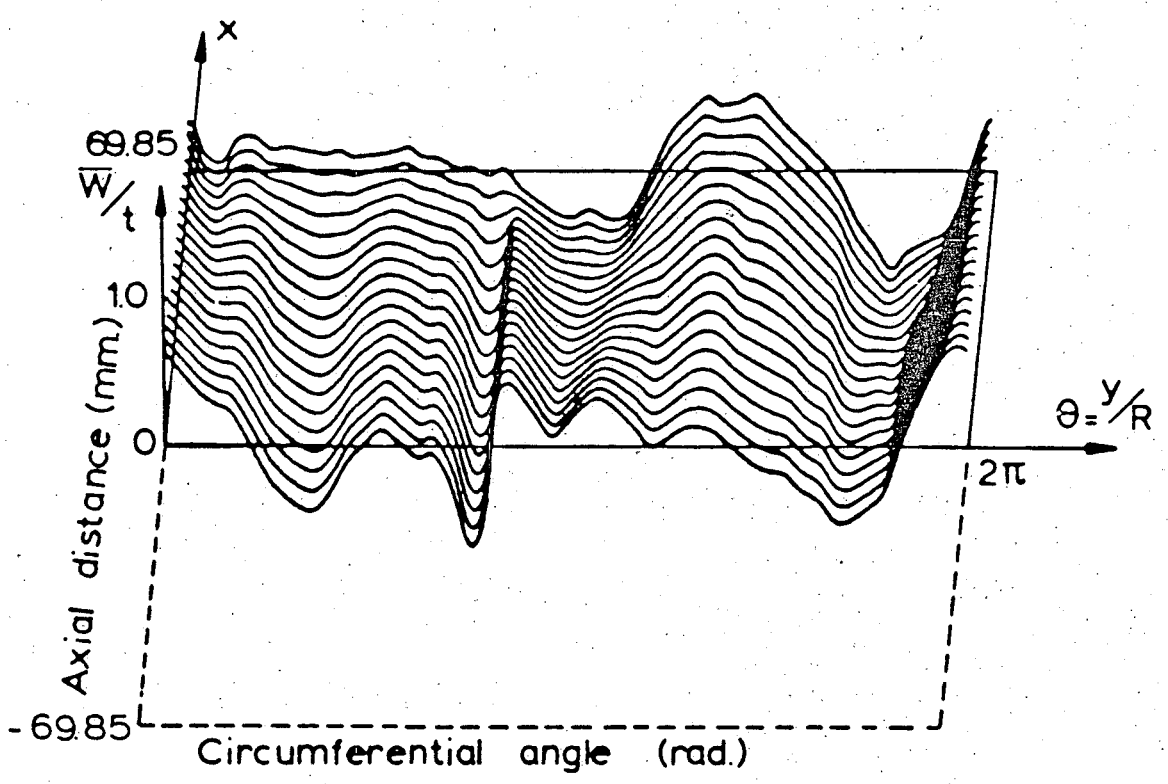

Fig.13 Cubic spline fitted initial shape of the upper half of the stringer stiffened shell AS-2

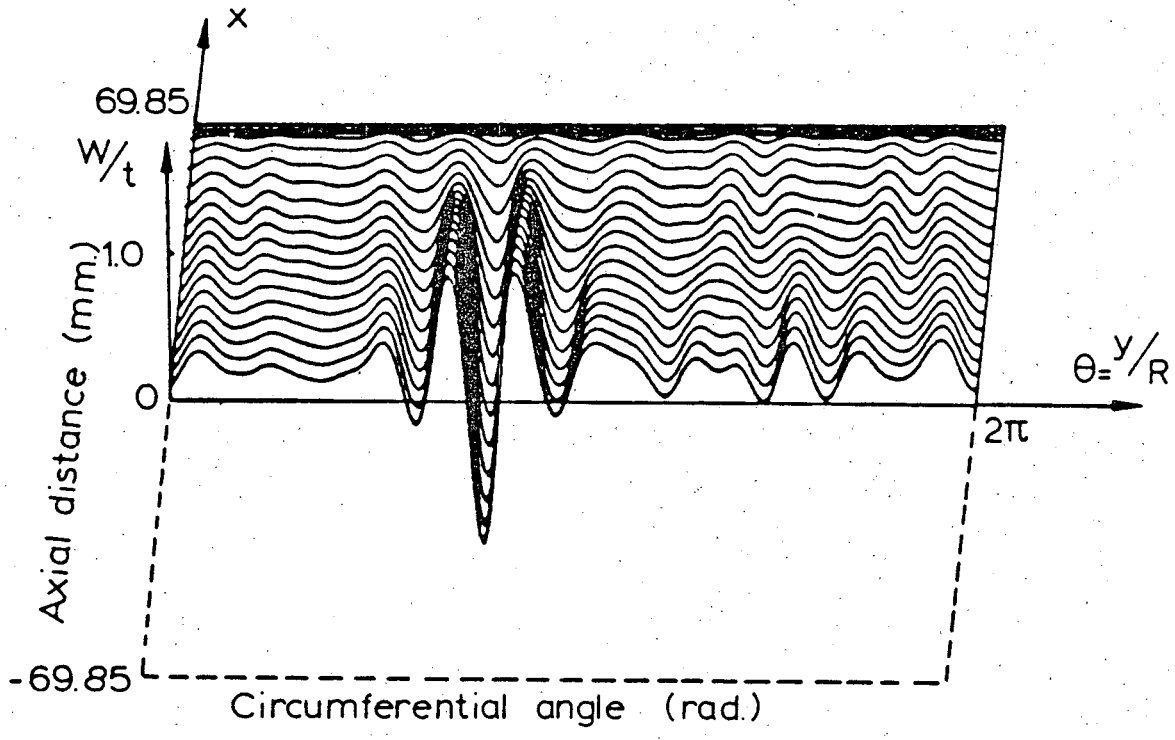

Fig.14 Calculated prebuckling deformation at the limit point $\rho_s = 0.84101$

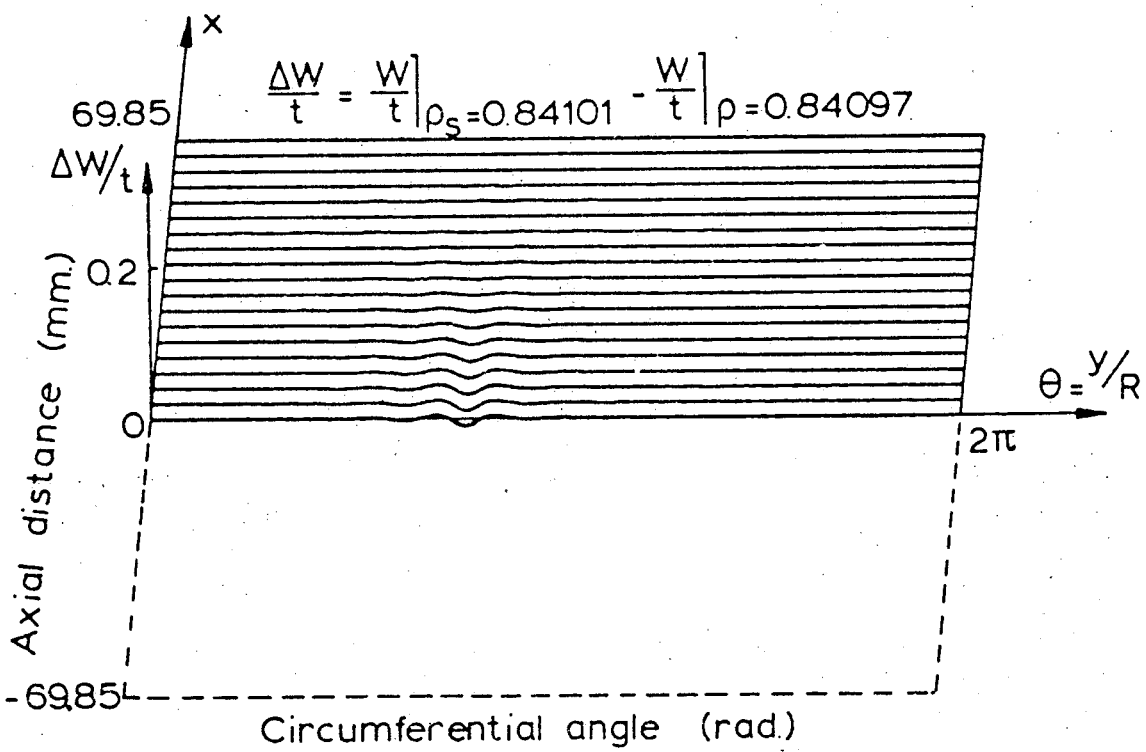

Fig.15 Calculated collapse mode at $\rho_s = 0.84101$

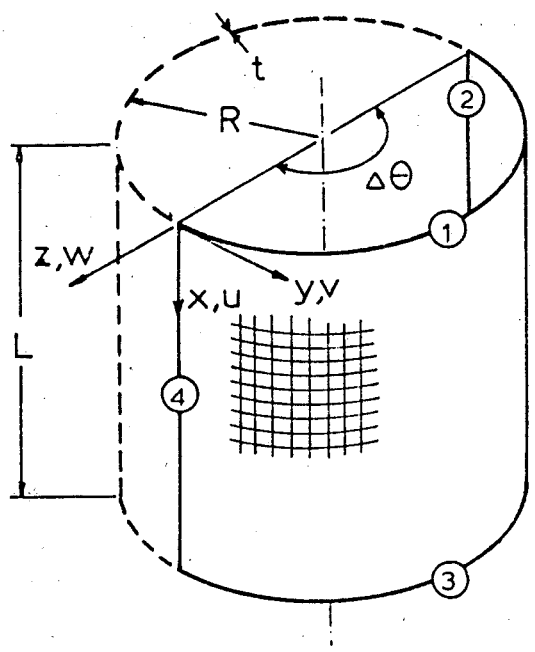

Boundary conditions

① $u \neq 0$, $v = w = w_{,x} = 0$

②, ④ symmetry

③ $u = v = w = w_{,x} = 0$

$\Delta\theta = 180°$

Fig.16 Shell segment used for collapse analysis of imperfect shells (Discrete model C)

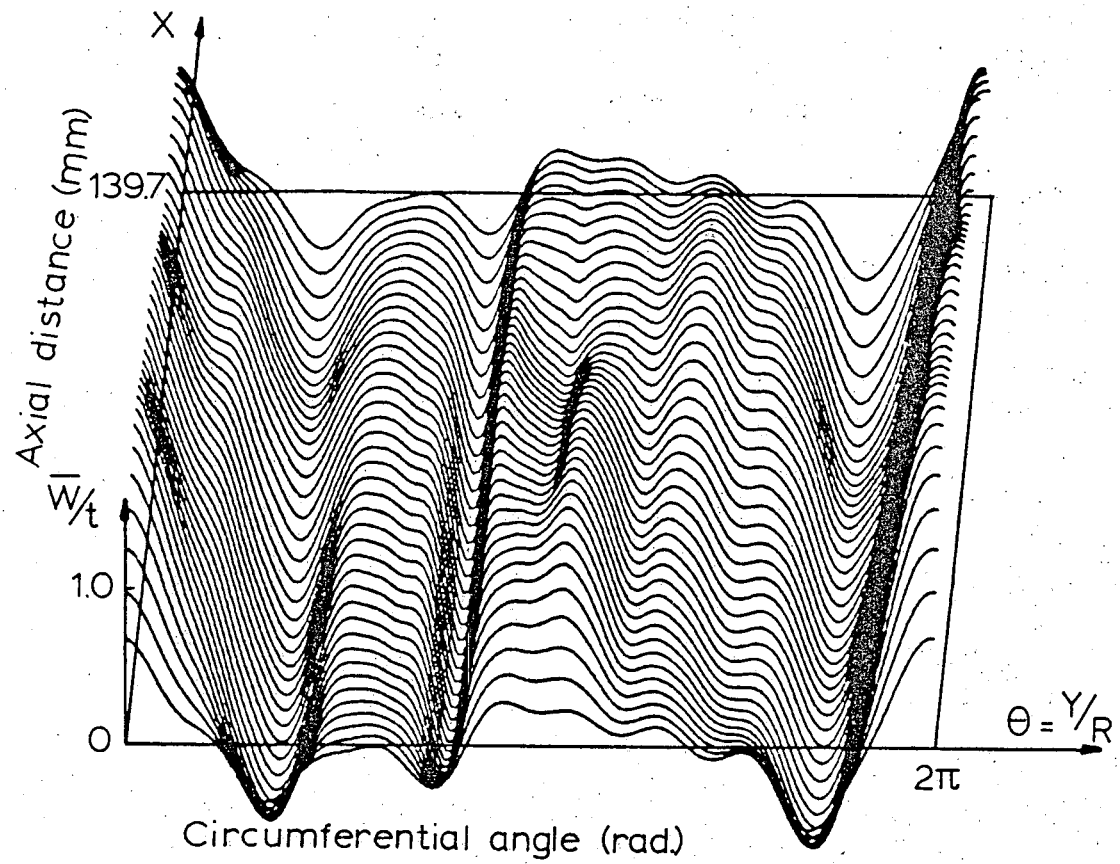

Fig.17 Recomputed initial shape of the stringer stiffened shell AS-2 using 132 Fourier coefficients

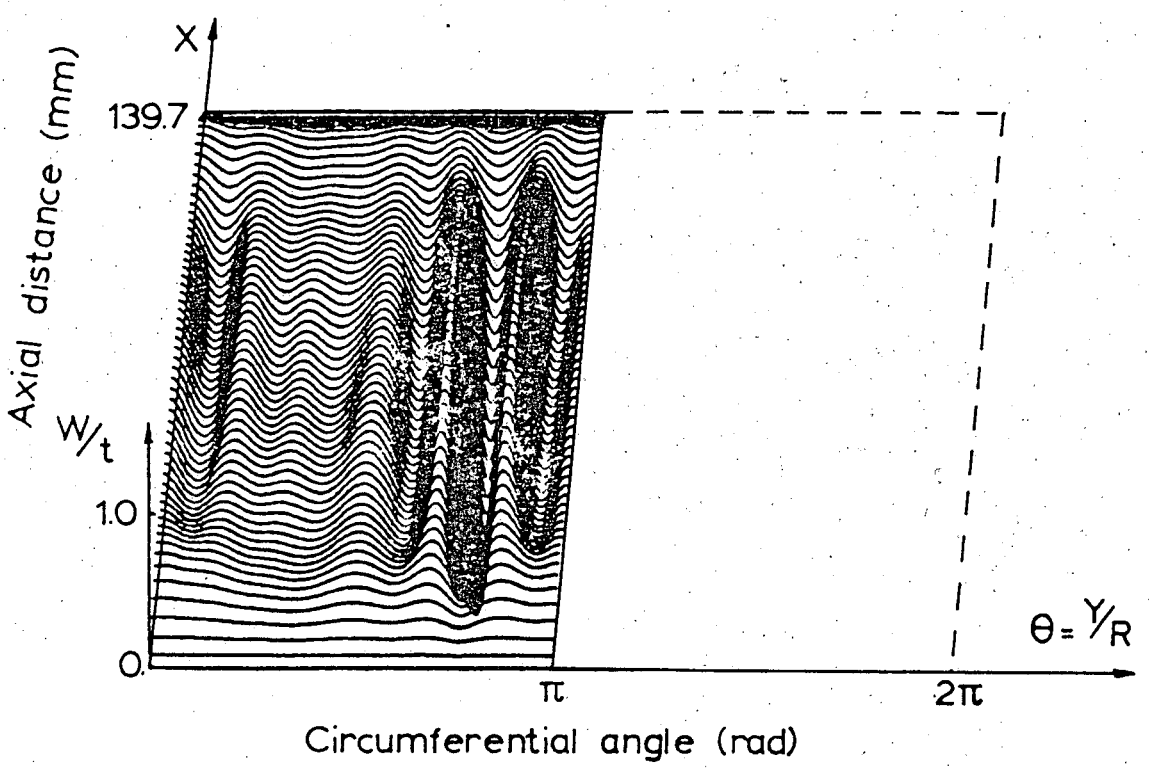

Fig.18 Calculated prebuckling growth of the stringer stiffened shell AS-2 at $\rho = 0.78619$ (61 x 161 = 9821 mesh points) (Boundary conditions: $u = v = w = w_{,x} = 0$)

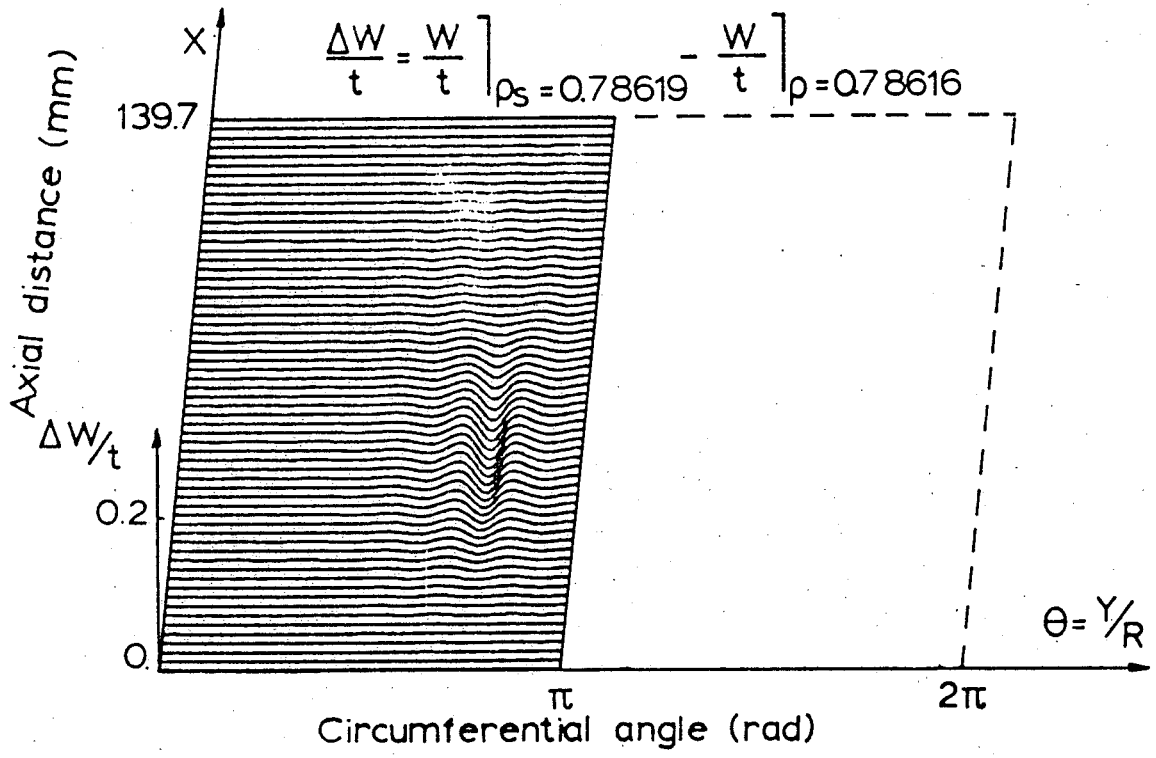

Fig.19 Calculated collapse mode of the stringer stiffened shell AS-2 at $\rho_s = 0.78619$ (61 x 161 = 9821 mesh points) (Boundary conditions: $u = v = w = w_{,x} = 0$)

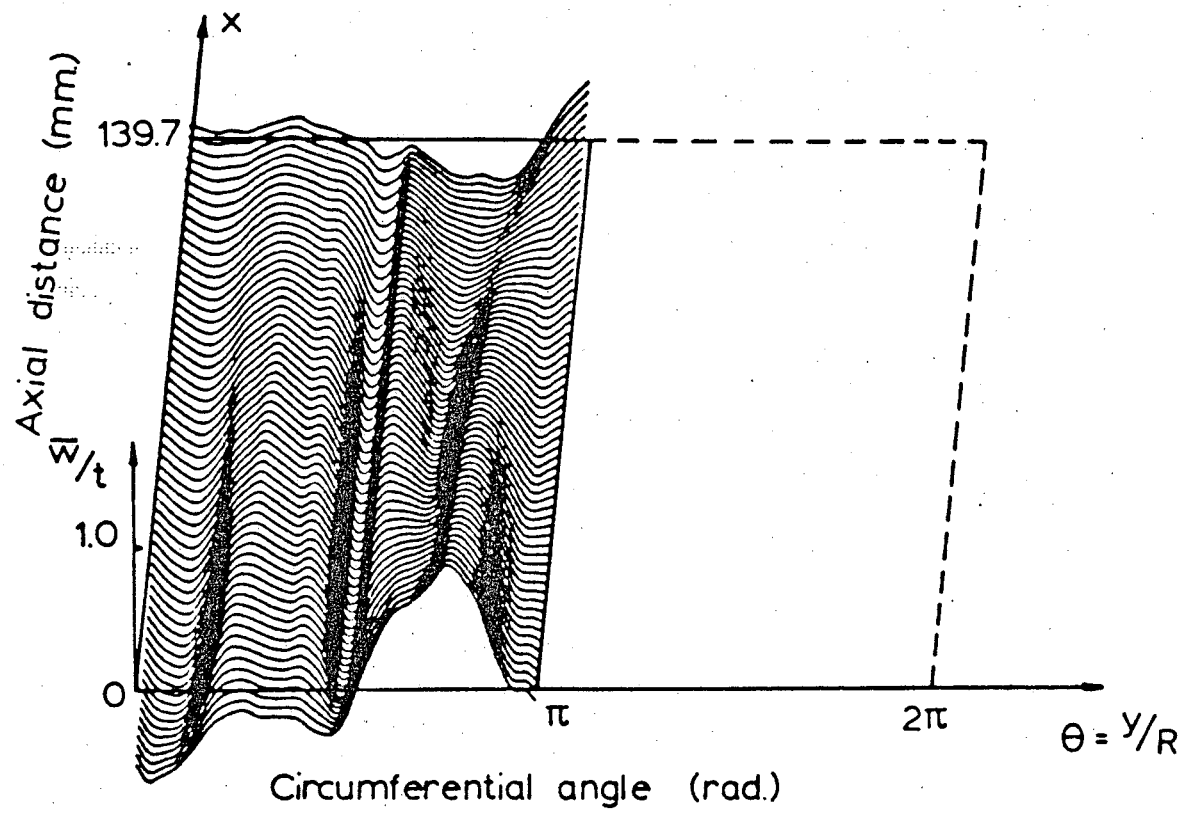

Fig.20 Cubic spline fitted initial shape of the stringer stiffened shell AS-2 (61 x 161 = 9821 mesh points)

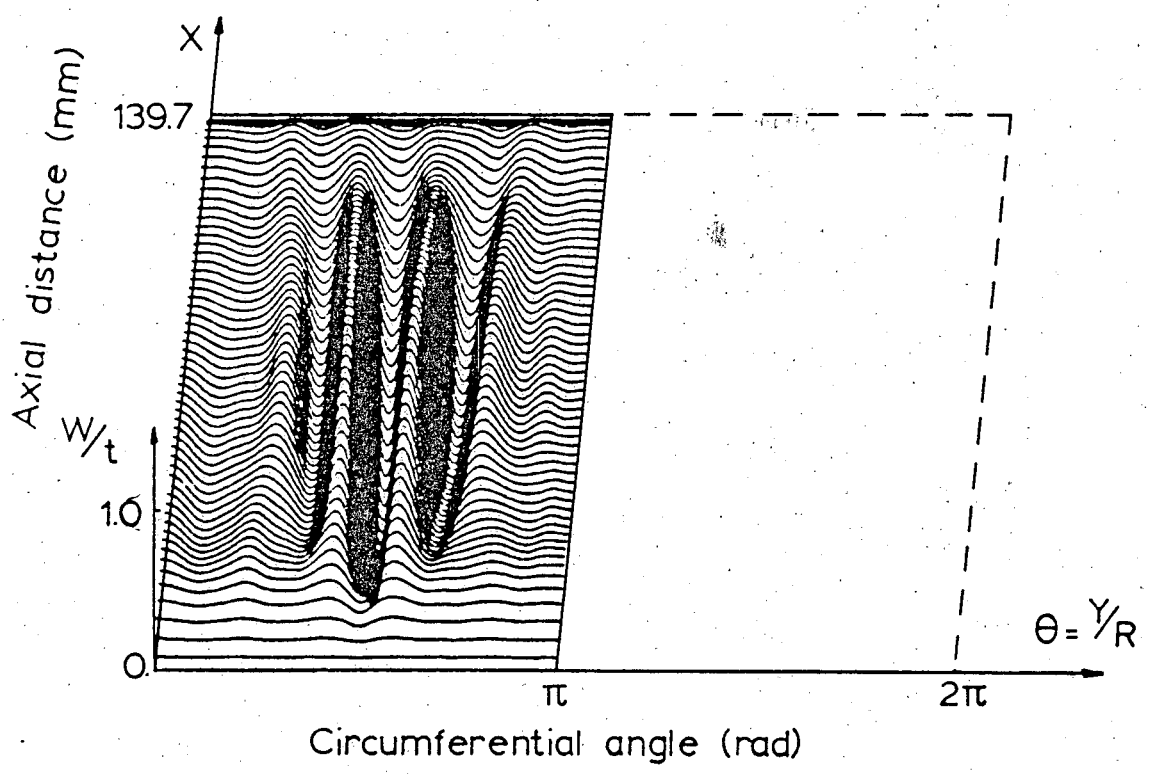

Fig. 21 Calculated prebuckling growth of the stringer stiffened shell AS-2 at $\rho_s = 0.8727$ (61 x 161 = 9821 mesh points) (Boundary conditions: $u = v = w = w_{,x} = 0$)

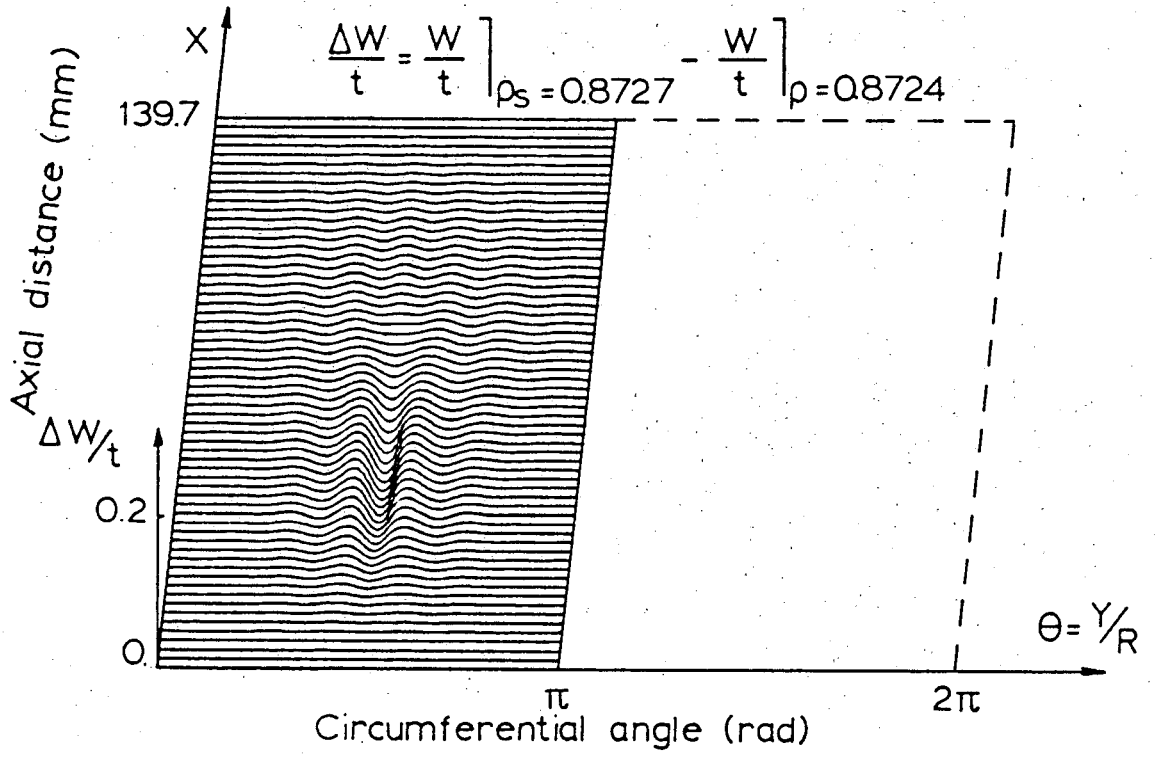

Fig. 22 Calculated collapse mode of the stringer stiffened shell AS-2 at $\rho_s = 0.8727$ (61 x 161 = 9821 mesh points) (Boundary conditions: $u = v = w = w_{,x} = 0$)

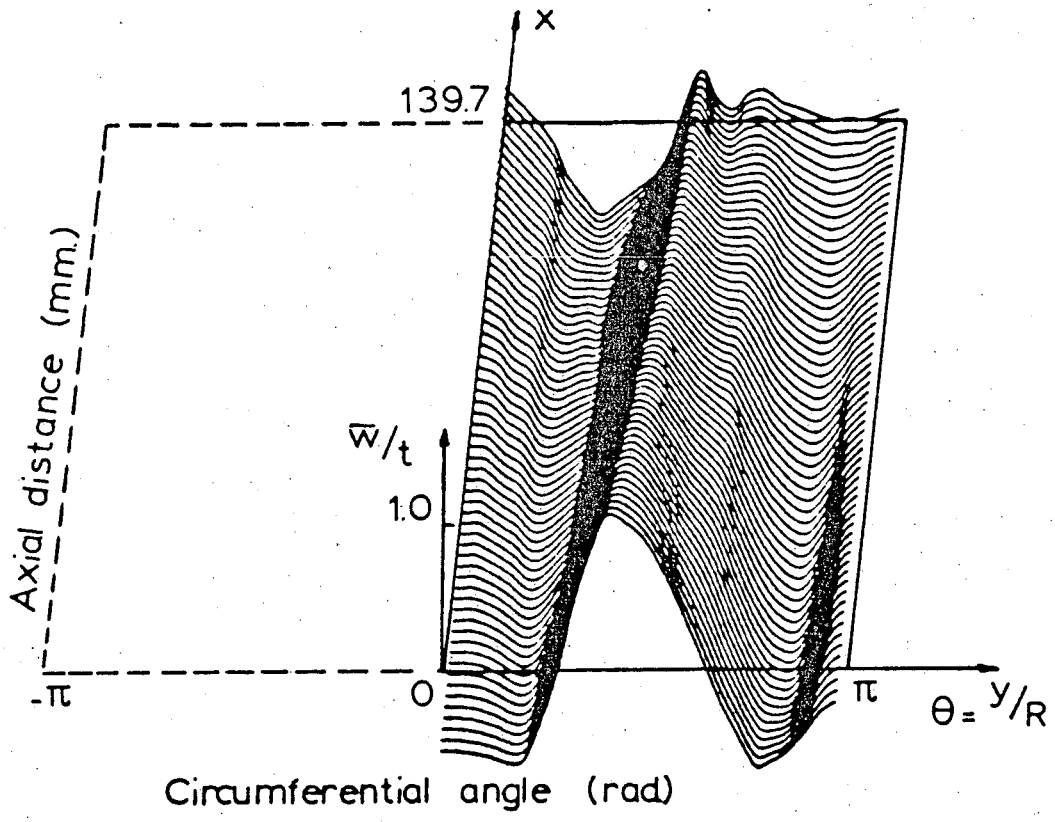

Fig. 23 Cubic spline fitted initial shape of the stringer stiffene shell AS-2 (61 x 161 = 9821 mesh points)

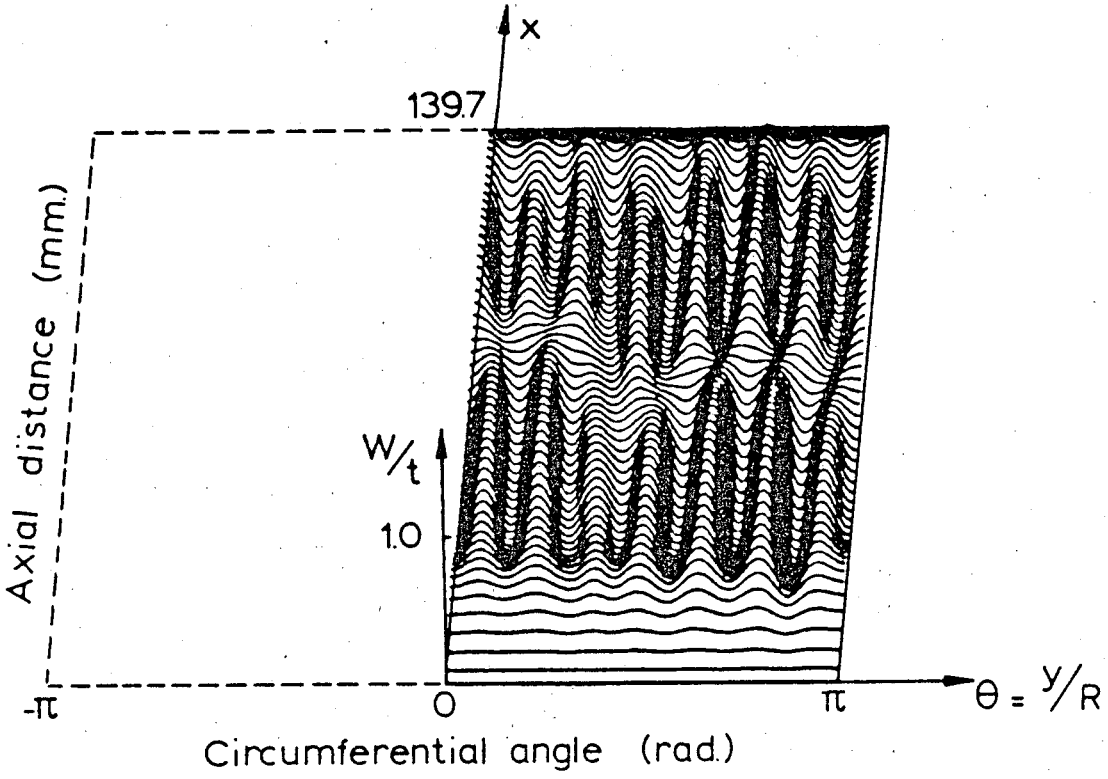

Fig. 24 Calculated prebuckling deformation at the limit point $\rho_s = 0.9513$

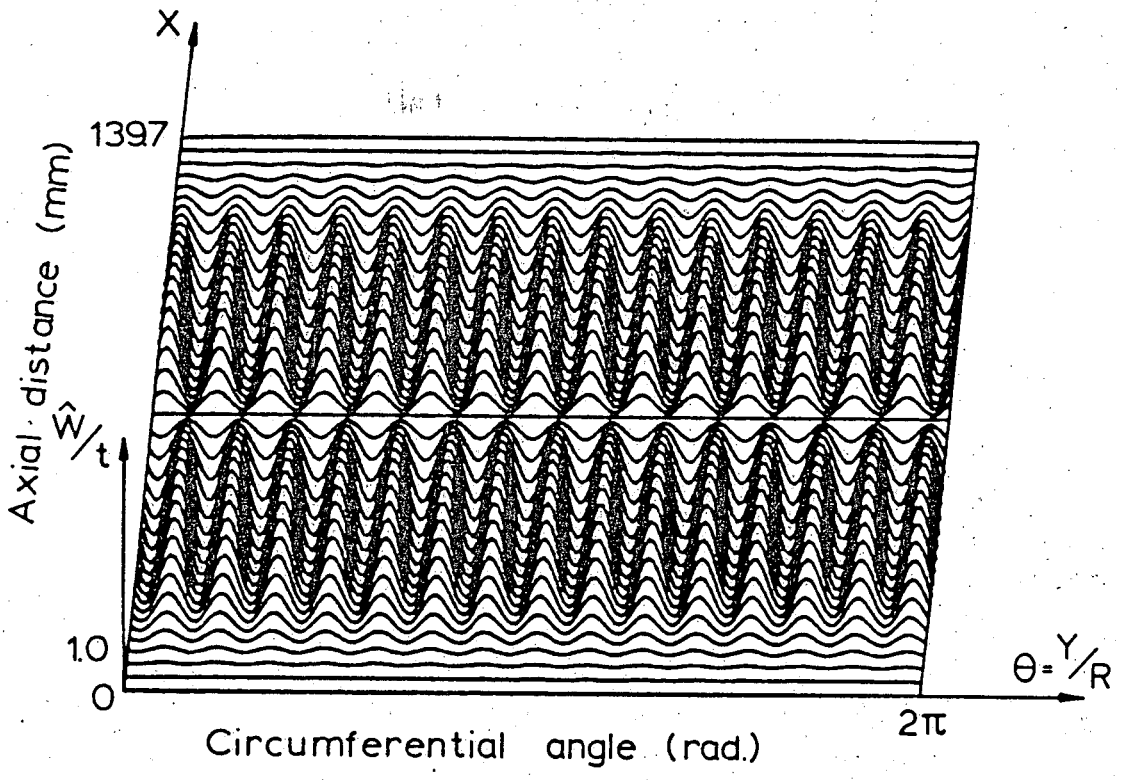

Fig.25 Bifurcation buckling mode of the stringer stiffened shell AS-2 (41×161=6601 mesh points $N_{BIF} = -308.80\ ^{N}/_{cm}$)
(Boundary conditions: $u = v = w = w_{,x} = 0$)

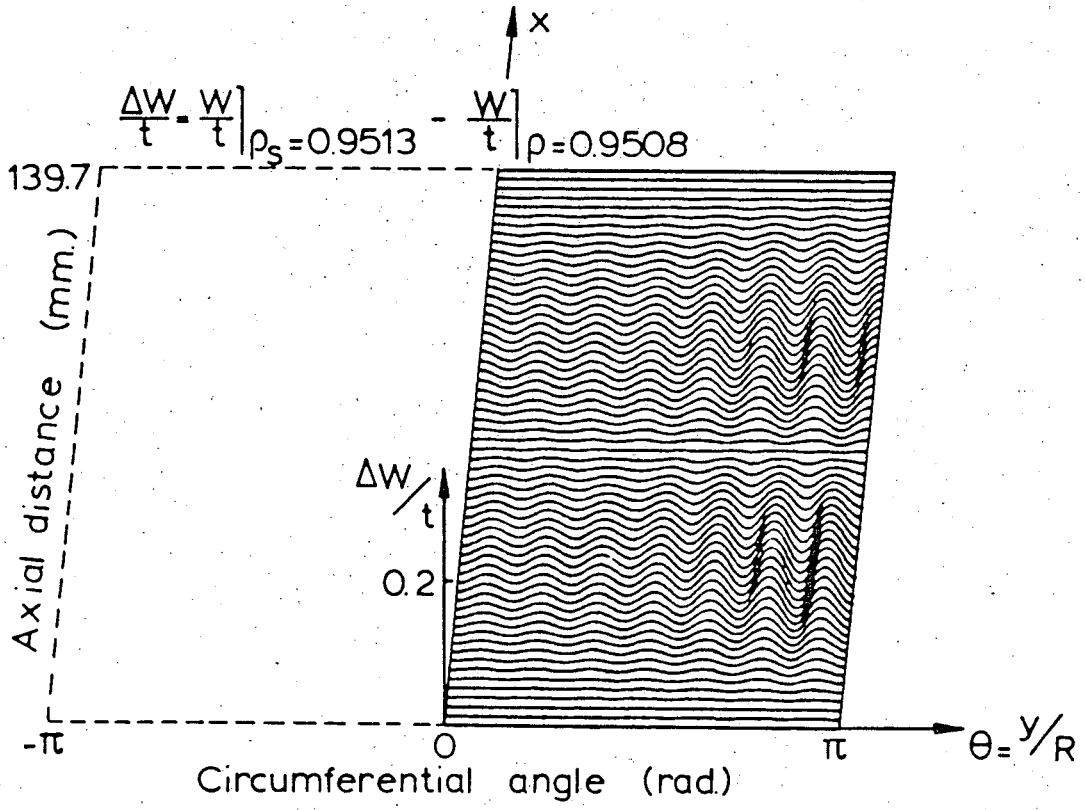

Fig. 26 Calculated collapse mode at $\rho_s = 0.9513$

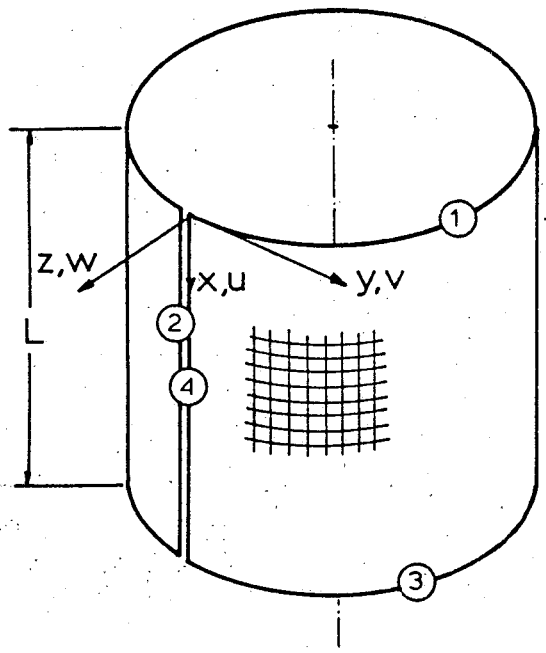

Boundary conditions

① $u \neq 0$, $v = w = w_{,x} = 0$

②, ④ displacement compatibility

③ $u = v = w = w_{,x} = 0$

$\Delta\theta = 360°$

Fig.27 Shell segment used for collapse analysis of imperfect shells (Discrete model D)

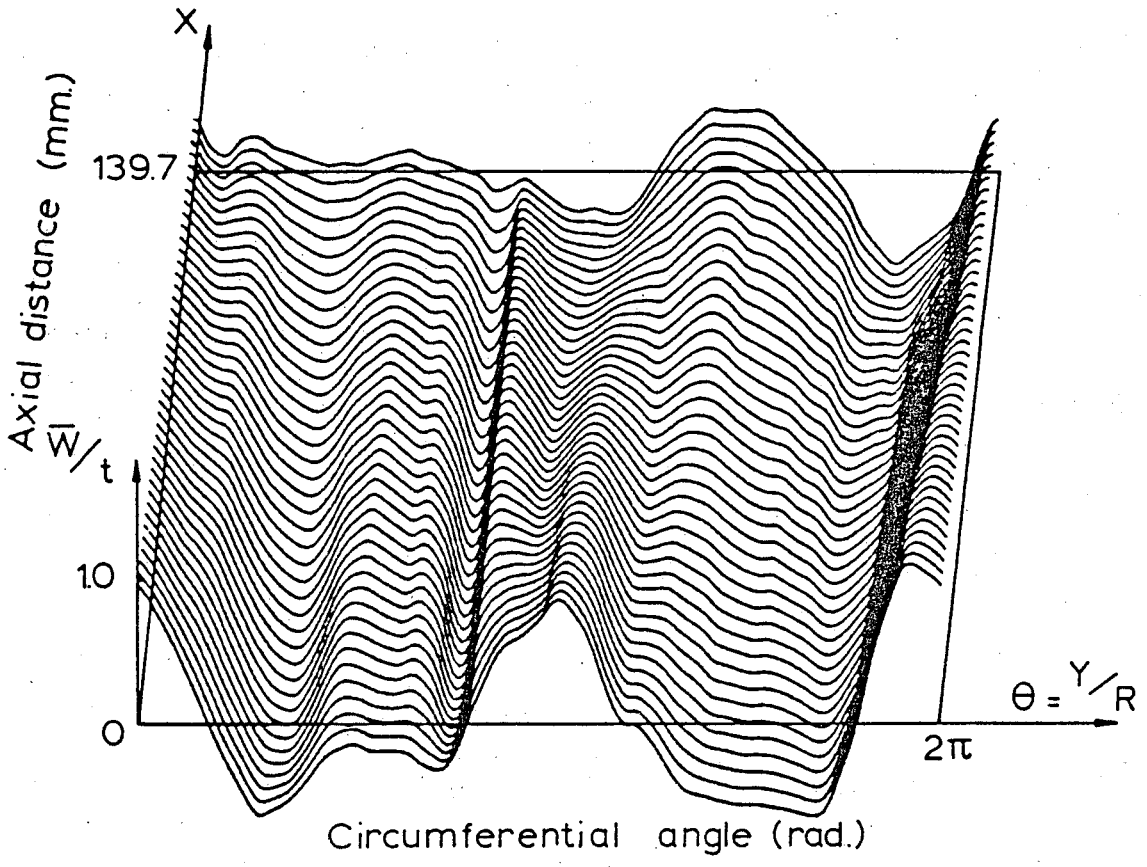

Fig.28 Cubic spline fitted initial shape of the stringer stiffened shell AS-2 (41x161=6601 mesh points)

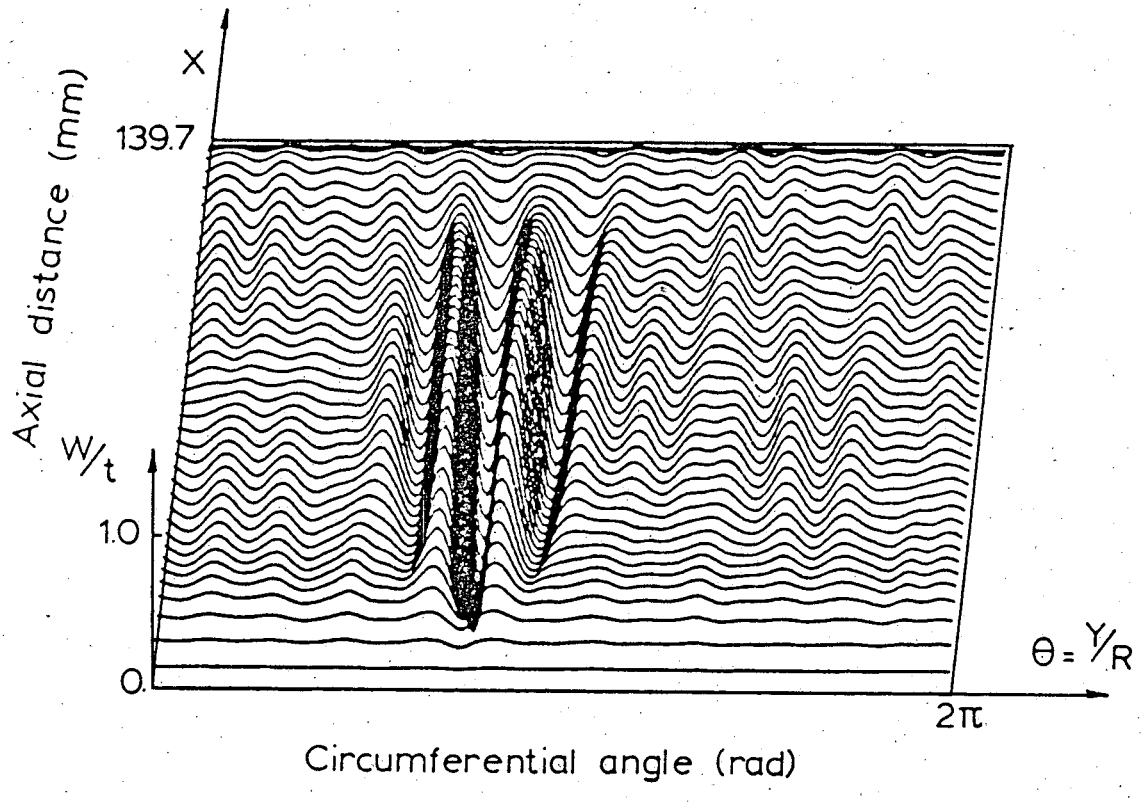

Fig. 29 Calculated prebuckling growth of the stringer stiffened shell AS-2 at $\rho_s = 0.8563$ (41 x 161 = 6601 mesh points) (Bcundary conditions: $u = v = w = w_{,x} = 0$)

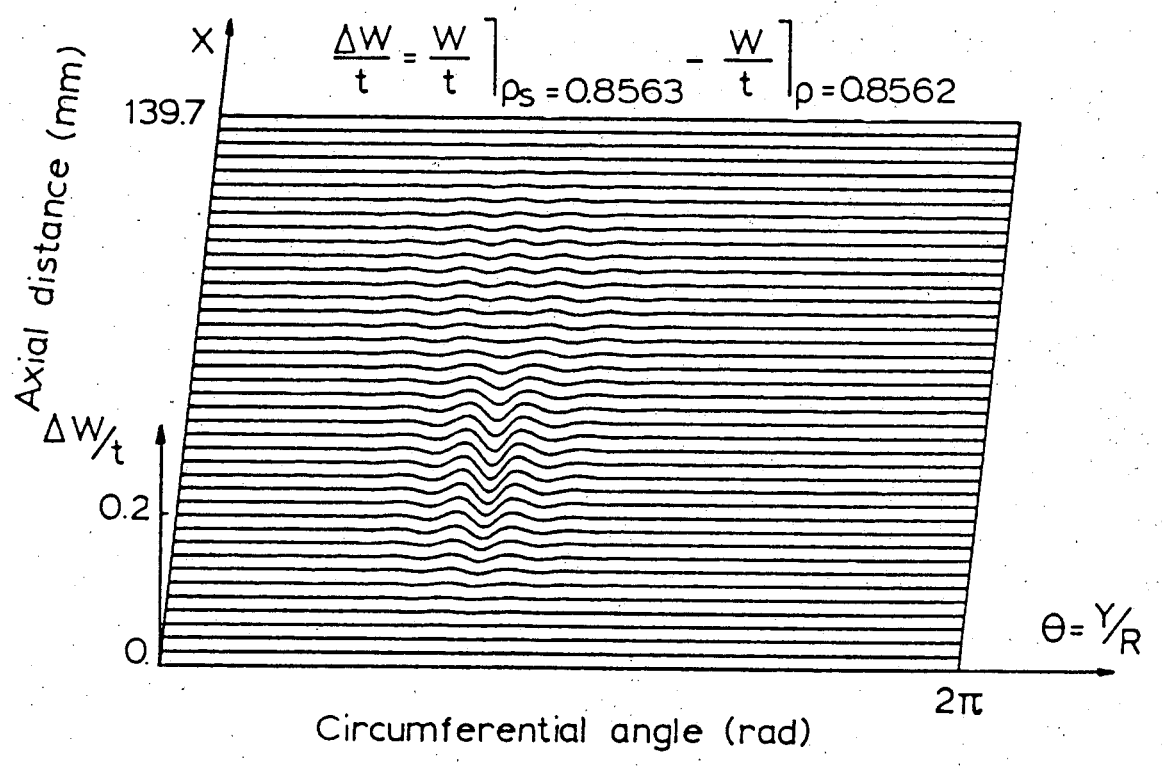

Fig. 30 Calculated collapse mode of the stringer stiffened shell AS-2 at $\rho_s = 0.8563$ (41 x 161 = 6601 mesh points) (Boundary conditions: $u = v = w = w_{,x} = 0$)

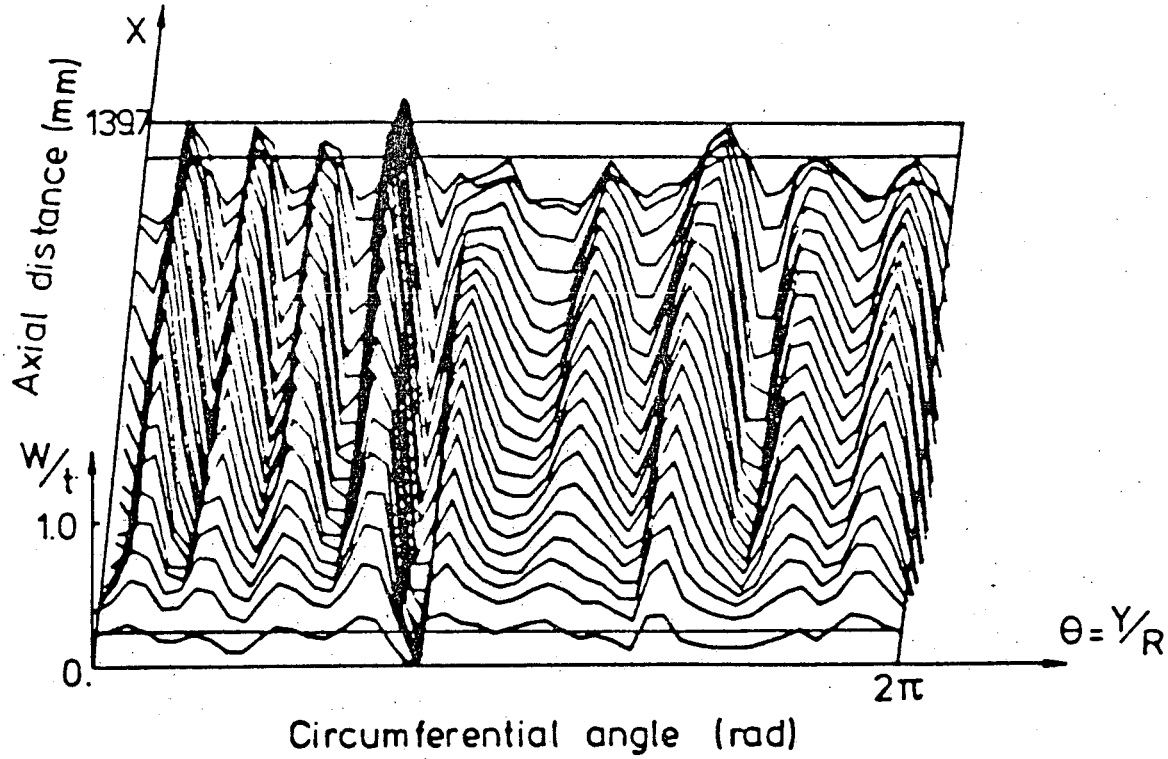

Fig.31 Measured prebuckling growth of the stringer stiffened shell AS-2 at $\rho=0.629$ ($21\times49=1029$ data points)

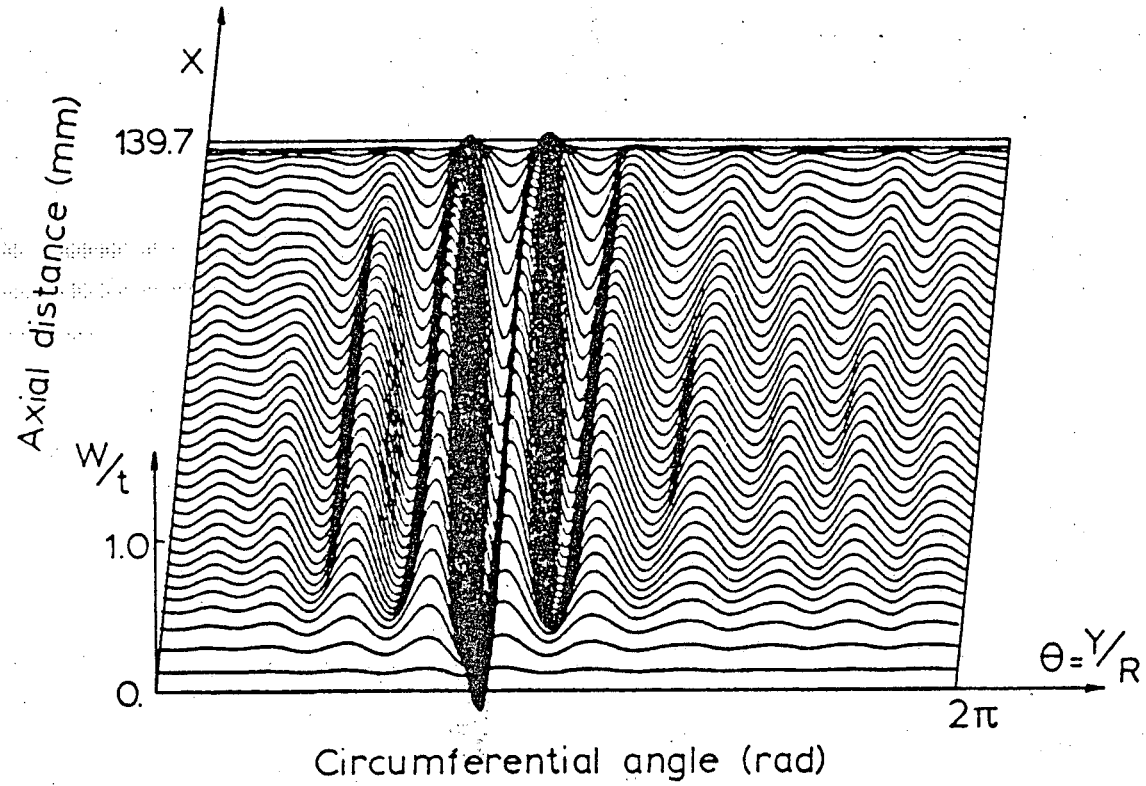

Fig.32 Calculated prebuckling growth of the stringer stiffened shell AS-2 at $\rho_s=0.8153$ ($41\times161=6601$ mesh points) (Boundary conditions: $N_x=v=w=w_{,x}=0$)

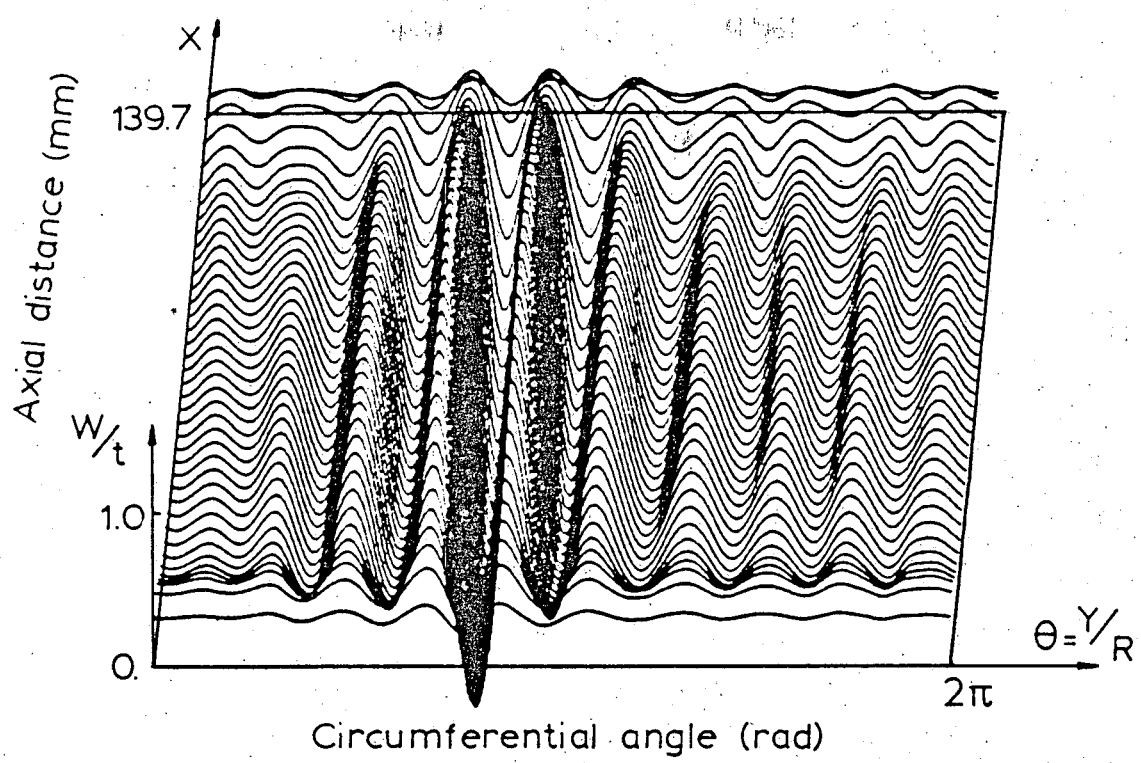

Fig.33 Calculated prebuckling growth of the stringer stiffened shell AS-2 at $\rho_s = 0.8095$ (41 x 161 = 6601 mesh points) (Boundary conditions: $N_x = v = w = M_x = 0$)

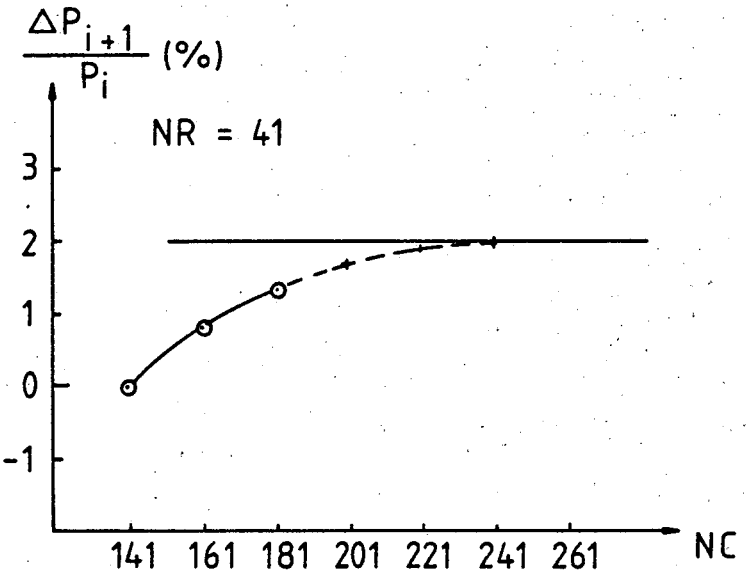

Fig. 34 Convergence behaviour of the collapse analysis of a complete shell